Research Square

Preprints are preliminary reports that have not undergone peer review.
They should not be considered conclusive, used to inform clinical practice,
or referenced by the media as validated information.

The Ketogenic Diet Ameliorates Nitroglycerin-Induced Chronic Migraine in Mice via Modulation of the Gut-Brain Axis

Jiali Zhang
Lanzhou University Second Hospital
Lei Wang
Lanzhou University Second Hospital
Liming Fan
Lanzhou University Second Hospital
Jifei Liu
Lanzhou University Second Hospital
ZhengHui Kang
Lanzhou University Second Hospital
Yibo Wang
Lanzhou University Second Hospital
Chang Ge
Lanzhou University Second Hospital
Gang Su
Lanzhou University
Yonggang Wang
Capital Medical University
Zhenchang Zhang
tougao138936475950163.com

Lanzhou University Second Hospital

Research Article

Keywords: Chronic migraine, Central sensitization, Ketogenic diet, Gut microbiota

Posted Date: November 26th, 2026

DOI: https://doi.org/10.21203/rs.3.rs-11793279/v1

License: This work is licensed under a Creative Commons Attribution 4.0 International License.
Read Full License

Additional Declarations: No competing interests reported.

The Ketogenic Diet Ameliorates Nitroglycerin-Induced Chronic Migraine in Mice via Modulation of the Gut-Brain Axis

Jiali Zhang[1#], Lei Wang[1#], Liming Fan[1], Jifei Liu[1], ZhengHui Kang[1], Yibo Wang[1], Chang Ge[1], Gang Su[2*] Yonggang Wang[3*] and Zhenchang Zhang[1*]

Affiliation:

[1] Department of Neurology, The Second Hospital of Lanzhou University, Gate, No. 82 Linxia Road, Chengguan District, Lanzhou 730000, China.

[2] Institute of Genetics, School of Basic Medical Sciences, Lanzhou University, Lanzhou, Gansu, China.

[3] Headache Center, Department of Neurology, Beijing Tiantan Hospital, Capital Medical University, No.119 South Fourth Ring West Road, Fengtai District, Beijing 100070, China.

 # Contributed equally

*** Corresponding Author:** Gang Su, sugang@lzu.edu.cn, Yonggang Wang, w100yg@gmail.com, Zhenchang Zhang, tougao13893647595@163.com.

Abstract

Background: Clinical evidence suggests that the ketogenic diet (KD) has a certain interventional effect on chronic migraine (CM). However, the specific mechanisms of KD in alleviating CM remain unclear. Gut microbiota dysbiosis and the gut-brain axis (GBA) are implicated in the pathophysiology of CM. Therefore, this study aims to elucidate the specific mechanisms underlying the ameliorative effects of the KD on CM.

Methods: Eight-week-old male mice were progressively adapted to KD, after which repeated nitroglycerin (NTG) injections were administered to establish the CM model. Behavioral assessments were performed to determine the nociceptive thresholds. In the trigeminal nucleus caudalis (TNC), immunofluorescence was used to measure c-Fos and calcitonin gene-related peptide (CGRP) expression and examine microglial morphology. Gut microbiota composition was characterized through 16S rRNA sequencing. Intestinal Retrograde PRV-CAG-mRFP tracing was performed to delineate anatomical connections along the GBA. Hypothalamic RNA sequencing and immunofluorescence were then applied to assess transcriptomic alterations, neuronal hyperexcitability, and oxytocin (OT) expression in the hypothalamic paraventricular nucleus (PVN). Finally, Spearman's correlation analysis was conducted to examine the relationships between signature taxa and pathophysiological parameters.

Results: KD intervention alleviated hyperalgesia and suppressed c-Fos and CGRP overexpression, alongside microglial activation in the TNC. In the gut microbiota, KD reversed the NTG-induced increase in *Ligilactobacillus* and enriched *Akkermansia muciniphila* abundance. Notably, neural projections were identified between the ascending colon and the PVN. Within the PVN, KD attenuated abnormal neuronal excitability and aberrant OT expression.

Conclusions: The KD ameliorated hyperalgesia and central sensitization in CM mice. The underlying mechanism may involve modulating gut microbial

composition to partially reverse NTG-induced microbial dysbiosis, thereby attenuating neuronal hyperexcitability and aberrant OT expression within the PVN. These findings highlight the potential of KD as a lifestyle intervention for preventing the onset of CM.

Keywords: Chronic migraine; Central sensitization; Ketogenic diet; Gut microbiota

Graphical Abstract

Introduction

Chronic migraine (CM) is a common central nervous system (CNS) disorder. According to estimates from the 2021 Global Burden of Disease (GBD) study, the global prevalence of CM is 15.2% (18.9% in females and 11.4% in males). Notably, the study highlighted that CM ranks second among all diseases globally in terms of years lived with disability (second only to major depressive disorder)[1]. The primary clinical manifestations of CM include unilateral, pulsating, or distending headaches, which are frequently accompanied by various reversible symptoms such as photophobia, phonophobia, cutaneous allodynia, nausea, and vertigo[2]. Furthermore, CM patients frequently present with gastrointestinal comorbidities—such as irritable bowel syndrome (IBS), inflammatory bowel disease (IBD), and celiac disease—at a rate significantly higher than that in the general population. Many patients also report gastrointestinal symptoms, including nausea and vomiting, during CM attacks, suggesting an intrinsic link between gastrointestinal function and CM[3–5]. In a

previous study, Li et al. found that germ-free(GF) mice (without gut microbial colonization) exhibited enhanced basal mechanical sensitivity but failed to develop further hyperalgesia following nitroglycerin (NTG) administration. Restoration of the gut microbiota reversed both basal mechanical hyperalgesia and the blunted response to NTG, indicating that an intact gut microbiome is required for normal nociceptive processing[6]. Additionally, mice transplanted with the gut microbiota profile of CM patients exhibited more severe hyperalgesia compared to those receiving microbiota from matched healthy controls. This demonstrates that susceptibility to NTG-induced CM-like attacks can be transferred from patients to mice via fecal microbiota transplantation (FMT)[7]. Moreover, in NTG-induced CM mouse models, the administration of short-chain fatty acids (SCFAs), such as sodium propionate (SP) and sodium butyrate (SB), mitigated tissue damage in the trigeminal nucleus caudalis (TNC), decreased the expression of pro-inflammatory mediators, and alleviated CM attacks[8]. Within the intestinal tissues, SCFA treatment was also found to significantly reverse mucosal alterations and concurrently promote the release of neurotransmitters in the enteric nervous system[9].

The gut microbiome and CM are interconnected through bidirectional relationships[10]. NTG-induced CM can lead to gut dysbiosis, which in turn affects the structure of the gut microbiome and its metabolic pathways. Notably, shifts were observed in the relative abundances of *Akkermansia muciniphila*, *Lachnospiraceae*, and related metabolites[11, 12]. Similarly, CM models

induced by inflammatory soup (IS) show marked differences in gut microbial composition and metabolite profiles when comparing CM-affected rats to healthy ones[13]. These observations highlight the close link between gut microbes, their metabolites, and CM development.

In addition to pharmacological approaches, nutritional strategies have gained increasing attention for the prevention and treatment of CM in recent years[14]. The ketogenic diet (KD) is a specialized metabolic intervention. Clinical evidence shows that KD reduces the frequency and duration of CM. It also decreases the patient's reliance on analgesics[15, 16]. Furthermore, KD demonstrates neuroprotective potential in various CNS diseases. In CNS diseases, KD remodels neuronal energy metabolism and cellular homeostasis[17]. It counteracts oxidative stress and downregulates proinflammatory cytokines[18]. KD also balances neurotransmitters to suppress abnormal cortical excitability[19]. These mechanisms have been well established in other CNS disorders. These findings provide important clues regarding the neuroprotective role of the KD. However, the specific pathways of KD in treating CM remain unclear. Recently, the gut-brain axis (GBA) has become a crucial link between the gut microbiota and the CNS. GBA plays a prominent role in regulating central inflammation and neuronal excitability. Therefore, this study focused on the KD-induced remodeling of the gut microbiota. We aimed to explore whether altered microbiota composition can inhibit central sensitization via the GBA. To investigate this, we established a

CM mouse model using repeated NTG administration. This study sought to determine the effects of KD on the gut microbiota and clarify its mechanisms in alleviating CM. Ultimately, our findings provide a solid experimental and theoretical basis for microbiota-targeted dietary or probiotic interventions in future CM management.

Materials and methods

Animals

All animal experiments were approved by the Animal Ethics Committee of Lanzhou University Second Hospital, and were strictly carried out following the norms of the Institutional Animal Care and Use Committee (Ethics Number: D2025-900). The sample size of this study was determined based on previous related experiments. The 8-week-old male C57BL/6 J mice (body weight 20±2 g) used in this experiment were purchased from the Experimental Animal Center of Lanzhou Veterinary Research Institute. The mice were raised in the Experimental Animal Center of Lanzhou Veterinary Research Institute, and all animals were raised under standard conditions: 12-hour light/dark cycle and constant temperature environment. Before all experiments started, the mice were given a one-week experimental environment adaptation period.

CM mouse model

A CM mouse model was established via repeated intermittent intraperitoneal (i.p.) injections of NTG, a well-validated protocol widely adopted in previous studies[20]. A 5 mg/ml NTG stock solution (Beijing Yimin, China) was diluted in

0.9% saline and administered at a dose of 10 mg/kg via i.p. injection every other day for 9 days. The mice were randomly assigned to three groups: (A) vehicle (VEH) group: standard diet (SD) + saline; (B) NTG group: SD + NTG; and (C) KD + NTG group: KD + NTG. Following a one-week acclimatization period, the mice were maintained on either SD or KD for a total of 30 days. On day 21 of dietary intervention, the NTG administration protocol was initiated to establish the CM model. All mice were provided with nutritionally balanced diets formulated by Jiangsu Medisen Biomedical Co., Ltd.

Behavioral tests

All behavioral tests were conducted in a quiet environment between 8:00 AM and 3:00 PM. Prior to testing, mice were habituated to the testing environment for 5 consecutive days, for at least 30 minutes per session. On days 1, 3, 5, 7, and 9, periorbital and hind paw mechanical withdrawal thresholds, as well as thermal nociceptive thresholds, were evaluated immediately before (basal threshold) and 2 hours after NTG or VEH administration (acute hyperalgesia).Mechanical thresholds were assessed using von Frey monofilaments (0.008–2 g) applied perpendicularly to the periorbital region following the classic up-and-down method. A positive response in periorbital testing was defined as rapid head withdrawal or brisk stroking of the face with the ipsilateral forepaw. For the hind paw mechanical threshold assessment, mice were placed on an elevated wire mesh platform enclosed in a transparent Plexiglas chamber (L*W*H: 10*7*7 cm) and habituated for 30 minutes prior to

testing. The von Frey monofilament stimulation was performed identically to the periorbital method. A positive response was defined as paw withdrawal, flinching, or licking. Mechanical nociceptive thresholds were ultimately calculated using an online tool available at https://bioapps.shinyapps.io/vonFrey-app/[21].

Thermal nociceptive thresholds were measured using a hot plate apparatus maintained at 55 °C, surrounded by a transparent Plexiglas enclosure (Hot/Cold Plate Tester; Yuyan Instruments, Shanghai, China). The latency to the first hind paw lick was recorded as the thermal threshold. A strict cutoff time of 30 s was imposed to avoid tissue damage.

16S rRNA gene sequencing

Fecal samples were submitted to Majorbio Bio-Pharm Technology Co., Ltd. (Shanghai, China) for 16S rRNA gene sequencing. Fecal microbial genomic DNA was extracted using a TIANGEN DNA extraction kit (TIANGEN Biotechnology, China). This was performed according to the manufacturer's instructions. DNA quality was evaluated via 1% agarose gel electrophoresis. The bacterial 16S rRNA gene was amplified from the V3-V4 region using PCR. Sequencing was performed on the Illumina NextSeq 2000 PE300 platform. Gut microbiota data were analyzed on the Majorbio Cloud Platform.

RNA-seq data processing

Total RNA was extracted using TRIzol reagent. This was performed according to the manufacturer's instructions. RNA purity and quantification were

evaluated using a NanoDrop 2000 spectrophotometer (Thermo Scientific, USA). RNA integrity was assessed using an Agilent 2100 Bioanalyzer (Agilent Technologies, Santa Clara, CA, USA). Transcriptome libraries were constructed using the VAHTS Universal V10 RNA-seq Library Prep Kit (Premixed Version). This step was performed according to the manufacturer's instructions. Transcriptome sequencing was performed by OE Biotech Co., Ltd. (Shanghai, China). Sequencing was conducted on the Illumina NovaSeq 6000 platform. Data were analyzed using R (v 4.5.3) and related packages (e.g., DESeq2).

Immunofluorescence staining

Following NTG administration on day 9, three to four mice randomly selected from each group were used for immunofluorescence staining. The mice were deeply anesthetized via intraperitoneal injection of 1% sodium pentobarbital and transcardially perfused with 0.9% saline, followed by 4% paraformaldehyde (PFA). Brain tissues were rapidly harvested and post-fixed in 4% PFA overnight. Subsequently, the brains were sequentially cryoprotected in 20% and 40% sucrose solutions until they sank to the bottom. The tissues were then embedded in Tissue-Tek O.C.T. compound (Sakura 4583), cut into 25μm thick sections using a cryostat (Leica CM1950), and stored at -20 °C in a cryoprotectant solution (0.28 M sucrose, 30% ethylene glycol, and 0.1 M PB). For staining, the brain sections were washed with 0.01 M phosphate-buffered saline (PBS), post-fixed with 4% PFA for 20 minutes, and washed again with

PBS. The sections were then blocked with 10% normal goat serum in PBS for 1 hour at 37 °C. Following the blocking step, the sections were incubated overnight at 4 °C with the following primary antibodies: rabbit anti-c-Fos (1:1000; ab222699, Abcam), mouse anti-calcitonin gene-related peptide (CGRP) (1:200; sc-57053, Santa Cruz), rabbit anti-Iba-1 (1:100; ab178846, Abcam), and rabbit anti-oxytocin (OT) (1:800; ab212193, Abcam). All primary antibodies were diluted in a buffer containing 0.01 M PBS, 1% goat serum, and 3% Triton X-100. After washing with PBS, the sections were incubated with secondary antibodies—goat anti-rabbit Alexa Fluor 488 (1:200; Zenbio) or goat anti-mouse Alexa Fluor 488 (1:200; Zenbio)—in the dark for 1 hour at 37 °C. The nuclei were counterstained with 4′, 6-diamidino-2-phenylindole (DAPI), and the sections were ultimately mounted with a 50% glycerol medium.

Images were acquired using an inverted microscope with identical exposure settings. Relevant brain regions were manually delineated using ImageJ, based on the Paxinos and Franklin mouse brain atlas (The Mouse Brain in Stereotaxic Coordinates, 2nd Edition). For quantitative analysis, three adjacent sections were selected from each mouse, and positively stained cells were counted using the ImageJ software.

Elisa

Blood samples were collected from the tail vein of mice to obtain serum. Briefly, after the mice were anesthetized and properly restrained, venous blood was drawn using an insulin syringe. The collected blood was allowed to clot at room

temperature for 60 minutes. Subsequently, the samples were centrifuged at 5000 rpm for 30 minutes at 4 °C to separate the serum and remove any residual insoluble debris. The resulting serum was carefully transferred to a fresh microcentrifuge tube. Serum OT levels were quantified using an OT ELISA kit (Cat. No. JL12594-48T; Jianglai Biotechnology, China) in strict accordance with the manufacturer's protocol.

Viral injection into the ascending colon

Mice were secured in a stereotaxic apparatus (RDW Life Science, China). Anesthesia was maintained with 1% isoflurane throughout the surgical procedure. The PRV-CAG-mRFP viral (a retrograde tracer virus capable of crossing multiple synaptic levels) vector was loaded into a beveled glass micropipette (Narishige, Japan), which was subsequently mounted onto the stereotaxic manipulator. The micropipette was connected to a 10-μL Hamilton microsyringe (Hamilton, USA) driven by a precision syringe pump (KD Scientific, USA). The viral suspension was injected at a rate of 25 nL/s, delivering 750 nL per submucosal injection site. Each animal received a total volume of 3 μL in the ascending colon. All surgical procedures were performed on a heating pad. Postoperatively, the mice were allowed to recover under an infrared heating lamp until they voluntarily relocated to the unheated side of the home cage. At 144 hours post-injection, the mice were euthanized for tissue harvesting.

Statistical analysis

Statistical analyses were performed using GraphPad Prism 10.1.2 and R for Windows (V 4.5.3). Data in the figures are presented as mean ± standard error of the mean (SEM). Normally distributed data were analyzed using one-way or two-way ANOVA. ANOVA was followed by Tukey's post hoc test. Non-normally distributed data were analyzed using the Mann-Whitney U test. Multiple groups of non-parametric data were analyzed using the Kruskal-Wallis H test. This was followed by Dunn's post hoc test. Statistical significance is indicated as *$p < 0.05$, $p < 0.01$, and ***$p < 0.001$.

Results

KD ameliorates NTG-induced hyperalgesia in CM mice

To investigate the therapeutic effects of KD on CM, mice were subjected to a 30-day dietary intervention with either SD or high-fat, low-carbohydrate KD (Fig. 1A). Body weight and blood ketone levels were monitored on days 0, 10, 20, and 30. We observed that in the KD-NTG group, blood ketone levels began to elevate by day 10 and were maintained at a stable state of ketosis on days 20 and 30 (Fig. 1B). Meanwhile, no significant differences in body weight were observed across the groups throughout the entire intervention period (Fig. 1C). These findings indicate that the KD successfully induced a sustained ketotic state in the mice without exerting any notable adverse effects on their normal growth. Subsequently, starting on day 21 of the dietary intervention, the CM mouse model was established via alternate-day injections of NTG. Behavioral evaluations were conducted immediately before (basal threshold) and 2 hours

after (acute hyperalgesia) each administration (Fig. 1D). The results revealed that repeated NTG injections induced a progressive exacerbation of hyperalgesia in the NTG group. However, the KD intervention significantly reversed this trend. Compared to the NTG group, the KD not only elevated the basal mechanical withdrawal thresholds of both the periorbital region and the hind paws in CM mice, but also attenuated NTG-induced acute mechanical hyperalgesia (Fig. 1E, F). Similarly, mice in the KD-NTG group exhibited a recovery of basal thermal thresholds and acute thermal hyperalgesia in the thermal nociceptive test (Fig. 1G).

KD blunts NTG-induced c-Fos and CGRP overexpression and microglial activation within the TNC

To explore how KD alleviates hyperalgesia in CM, we evaluated the expression levels of CGRP and the neuronal activation marker c-Fos in the TNC. Immunofluorescence revealed a significant upregulation of CGRP relative fluorescence intensity in the TNC of the NTG group (Fig. 2A, C). The number of c-Fos-positive cells also increased substantially (Fig. 2B, D). KD intervention reduced both the density of CGRP-immunoreactive fibers and the count of c-Fos-positive cells (Fig. 2A-D). These results suggest that KD suppresses neuronal hyperexcitability in the TNC of CM mice. This suppression mitigates central sensitization. Microglial activation is crucial for driving and maintaining central sensitization in CM. Therefore, we used specific Iba-1 labeling to quantify microglial distribution and morphological

changes in the TNC. Data showed a significant increase in the total number of Iba-1+ microglia in the NTG group. These cells exhibited a typical abnormal activated morphology. Specifically, they displayed significant somatic hypertrophy, shortened total process length, and decreased branch endpoints. In contrast, KD intervention reduced the total number of Iba-1+ cells and promoted their return to a resting state morphology. This restoration was characterized by somatic retraction, process elongation, and increased branching (Fig. 2E-I). Overall, these findings demonstrate that KD inhibits microglial overactivation in the TNC of CM mice.

KD remodels the gut microbiota in CM mice

Previous studies have demonstrated that patients with CM exhibit significant gut microbiota dysbiosis[22]. To evaluate the modulatory effects of KD on the gut microbiome in CM, we performed 16S rRNA sequencing and bioinformatics analysis on the bacterial composition of fecal samples from each group. The results indicated that KD intervention altered the α-diversity of the gut microbiota in CM mice (Fig. S1A-D). UpSet plot analysis revealed differences in microbial community composition, with the VEH, NTG, and KD-NTG groups harboring 71, 55, and 70 unique operational taxonomic units (OTUs), respectively. This suggests that the KD induced treatment-specific microbial remodeling (Fig. 3A). Principal coordinate analysis (PCoA) demonstrated spatial separation among the three groups. Unlike the more scattered distribution observed in the NTG group, samples within the VEH and

KD-NTG groups clustered more tightly together (Fig. 3B). Analysis of similarities (ANOSIM) further confirmed the differences in gut microbial community structure among the three groups (Fig. 3C). This indicated that the KD effectively modulated the β-diversity of the microbiota in CM mice.

At the phylum level, the microbial communities across all groups were predominantly composed of *Bacillota* and *Bacteroidota*. Compared to the VEH group, the gut microbiota of NTG mice exhibited an increased abundance of *Bacteroidota* and *Actinomycetota*, alongside a decrease in *Bacillota* and *Campylobacterota*. Following KD intervention, the relative abundance of *Bacillota* significantly recovered, accompanied by a corresponding decrease in *Bacteroidota*. Minor phyla, such as *Actinomycetota* and *Thermodesulfobacteriota*, also exhibited subtle modulatory changes (Fig. 3D). At the family level, the NTG group showed a highly significant decrease in the relative abundances of *Lachnospiraceae, Desulfovibrionaceae, Akkermansiaceae, and Oscillospiraceae*, whereas KD intervention reversed these alterations (Fig. S2A-F). Heatmap clustering and quantitative analysis of differentially abundant species at the genus level further demonstrated that the relative abundances of *Ligilactobacillus*, *Dubosiella*, and *Adlercreutzia* were elevated in the NTG group (Fig. 3E-F). KD intervention suppressed the overgrowth of these genera (Fig. 3G-I). Conversely, taxa such as *Faecalibaculum*, which were depleted in the NTG group, showed an increase in relative abundance following KD intervention (Fig. 3J).

LEfSe analysis was employed to identify the key signature taxa in each group. The VEH group was primarily characterized by *Muribaculaceae*, whereas the NTG group exhibited significant enrichment of *Lactobacillales*, *Ligilactobacillus*, and *Dubosiella*. In contrast, within the KD-NTG group, the abundance of *Ligilactobacillus* underwent a precipitous decline, which was supplanted by a highly significant enrichment of *Clostridia*, *Allobaculum*, *Faecalibaculum*, and various beneficial taxa *Lachnospirales* and *Oscillospirales* (Fig. 4A). To explore the potential interaction networks among gut bacteria under KD intervention, Spearman's correlation analysis was conducted to evaluate the interrelationships among the top 30 dominant genera based on relative abundance. The results revealed that *Ligilactobacillus* was significantly negatively correlated with most of the dominant bacteria, forming a robust ecological exclusion network (Fig. 4B). Furthermore, Kyoto Encyclopedia of Genes and Genomes (KEGG) pathway predictions based on PICRUSt2 and Tax4fun revealed pronounced shifts in the functional profiles of the gut microbiome. Compared with the KD-NTG group, functional gene clusters related to Cellular Processes and Environmental Information Processing were diminished in the NTG group, while those associated with overall Metabolism were enriched (Fig. 4C). Consistent with the characteristics of an extremely low carbohydrate intake, the KD suppressed the phosphotransferase system (PTS), which is responsible for carbohydrate absorption. Concurrently, key metabolic pathways involved in

354 neurotransmitter precursor synthesis and SCFAs generation, such as Pyruvate
355 metabolism and Biosynthesis of amino acids, also displayed differential
356 abundances across the experimental groups (Fig. 4D).

357 **Anatomical connectivity from the gut to the PVN**

358 To investigate the GBA mechanisms by which KD ameliorates CM, we first
359 traced the projection pathways from the gut to the CNS by injecting
360 PRV-CAG-mRFP into the intestinal walls of the mice' ascending colon (Fig.
361 5A). Immunofluorescence analysis clearly revealed prominent
362 PRV-CAG-mRFP signals within the hypothalamic paraventricular nucleus
363 (PVN). This demonstrated the existence of a direct neural projection pathway
364 from the gut to the PVN and providing a neuroanatomical basis for GBA
365 regulation (Fig. 5B). Subsequently, we evaluated the activation profile of these
366 gut-projecting neurons under the NTG-induced episodic migraine (EM) state.
367 We observed that a substantial number of PRV-labeled hypothalamic neurons
368 co-expressed c-Fos (i.e., c-Fos+/RFP+ cells, indicated in yellow). Quantitative
369 pie chart analysis indicated that approximately 37.4% of the gut-projecting
370 neurons were highly activated in this EM model (Fig. 5C). This suggests that
371 this gut-brain circuit is directly involved in the central sensitization process of
372 CM.

373 **KD remodels the hypothalamic transcriptomic profile in CM mice**

374 To further investigate the mechanisms by which KD attenuates central
375 sensitization and hyperalgesia, RNA sequencing (RNA-seq) was performed.

Transcriptomic analysis revealed distinct clustering and segregation of the samples among the VEH, NTG, and KD-NTG groups (Fig. 6A). The gene expression heatmap confirmed that the KD intervention broadly reversed the NTG-induced aberrant gene expression profiles at the transcriptional level (Fig. 6B). Furthermore, Gene Set Enrichment Analysis (GSEA) demonstrated that the KD intervention positively enriched for the "cellular response to peptide hormone stimulus" (Fig. 6C). The genes reversed by the KD were highly concentrated in the "neuropeptide signaling pathway", while metabolic pathways such as cholesterol biosynthesis and mitochondrial ATP synthesis were significantly downregulated. Subsequent KEGG and Gene Ontology (GO) functional enrichment analyses targeting these core KD-reversed genes revealed that they are primarily localized to the external side of the plasma membrane. These genes were enriched in pathways related to neuroactive ligand-receptor interactions, cholinergic synapses, and cadherin signaling. Moreover, they are broadly involved in key neuro-immune regulatory biological processes, including chloride transport, nerve impulse conduction, and homophilic cell adhesion (Fig. 6D, E). Taken together, these transcriptomic findings indicated that KD ameliorates hyperalgesia by comprehensively modulating the signaling networks associated with central sensitization.

KD suppresses neuronal hyperexcitability and restores OT homeostasis in the PVN

Building upon the RNA sequencing findings regarding the neuropeptide

signaling pathway, we further focused on the alterations of peptidergic neurons in the PVN. Immunofluorescence staining revealed a significant increase in the number of c-Fos-positive cells in the NTG group compared to the VEH group (Fig. 7A, C). This confirms the hypersensitization of the PVN as a pain integration center during CM attacks. Concurrently, we quantified serum OT levels and observed a marked elevation in CM mice; whereas the KD group exhibited a trend toward reduction, although this did not reach statistical significance (Fig. 7D). Subsequently, immunofluorescence was employed to assess OT expression within the PVN. The results showed that OT expression was significantly upregulated in the NTG model, but was attenuated following KD intervention (Fig. 7B, E). As a neuroendocrine factor, the aberrant hypersecretion of OT is considered a compensatory disorder during the CM state. The KD intervention significantly decreased c-Fos expression and mitigated the NTG-induced over-expression of OT. These findings demonstrate that KD does not merely act as a simple analgesic, but rather restores homeostasis in the PVN by modulating GBA signaling.

The KD attenuates neuroinflammation and central sensitization by enriching *Akkermansia muciniphila*

To further elucidate the potential mechanisms of KD in alleviating CM, we performed an in-depth analysis of gut microbiota characteristics at the species level. Consistent with previous studies, the relative abundance of *A. muciniphila* significantly decreased in male CM mice. KD intervention

effectively restored the abundance of this bacterium (Fig. 8A, B). Furthermore, co-occurrence network analysis demonstrated a synergistic symbiotic network. *A. muciniphila* co-occurred with *Bifidobacterium pseudolongum, Alistipes inops*, and the SCFA-producing *Faecalibaculum rodentium* (Fig. 8C). Spearman's correlation analysis further revealed a close relationship between specific microbiota and indicators of central sensitization. Specifically, *A. muciniphila* and *Ileibacterium valens* positively correlated with microglial branches and microglial endpoints. They negatively correlated with Iba-1+ cells, microglial soma size, c-Fos+, and oxytocin. Conversely, *Ligilactobacillus murinus* negatively correlated with microglial branches and microglial endpoints (Fig. 8D). The existing literature indicates that *A. muciniphila* protects the intestinal mucosal barrier and reduces intestinal inflammation. It also regulates neuroinflammation in CNS diseases, such as cognitive impairment and ischemic stroke[23–25]. In summary, KD may reverse the decreased abundance of *A. muciniphila* and synergistically regulate beneficial gut microbiota networks. This process alleviates migraine-related central sensitization.

Discussion

Currently, the age-standardized prevalence, incidence, and disability-adjusted life year (DALY) rates of CM show an upward trajectory[1]. It primarily affects young and middle-aged women. Clinical and preclinical studies have confirm significant alterations in the gut microbiota and its metabolites in CM. This

study demonstrates that KD exerts a protective effect against NTG-induced CM. The underlying mechanism primarily relies on the correction gut microbiota dysbiosis. It attenuates abnormal neuronal excitability and OT dysregulation in the PVN. Ultimately, this process blocks the progression of central sensitization.

The development of CM is typically accompanied by significant gut microbiota dysbiosis. In our study, NTG-induced CM mice exhibited an abnormal increase in specific genera compared to the VEH group. These included *Ligilactobacillus*, *Dubosiella*, and *Adlercreutzia*. Previous microbiota interventions in CM mostly focused on traditional beneficial bacteria like *Lactobacillus*. Clinical evidence shows that probiotic supplementation can alleviate CM attacks[26, 27]. However, the role of *Ligilactobacillus* in CM is rarely reported. This genus also belongs to the *Lactobacillaceae* family. Previous studies often consider *Ligilactobacillus* a potential beneficial bacterium. It can alleviate neuroinflammation and reverse metabolic syndrome and cognitive decline[28, 29]. However, in our CM mice, NTG intervention led to a significant enrichment of *Ligilactobacillus*. Furthermore, LEfSe analysis identified it as a characteristic biomarker for CM mice. This contradictory finding is not uncommon. Other studies have observed a significant expansion of *Ligilactobacillus* in Alzheimer's disease (AD) model mice. This expansion was closely related to the neuroinflammatory pathology of AD[30]. Therefore, the exact role of *Ligilactobacillus* in the CM pathophysiological network

remains unclear. It may act as a protective stress compensatory mechanism or a driver of neuroinflammation. Future mechanistic studies are needed to elucidate this. Following KD intervention, the abundance of *Ligilactobacillus* sharply decreased. This relieved competitive inhibition within the intestinal microenvironment and redistributed the survival space. This redistribution provided broad colonization space for *A. muciniphila*, which repairs the intestinal barrier. It also benefited beneficial SCFA-producing strains, such as *Faecalibaculum*, *Allobaculum*, and *Lachnospiraceae*. Previous CM microbiota studies reported that *Akkermansiaceae* is one of the most abundant taxa in VEH mice[11]. Consistent with previous KD studies, KD intervention in our study showed a trend towards restoring *A. muciniphila* levels ($p > 0.05$)[31]. This result may relate to the short intervention period or limited sample size. It could also stem from baseline differences in gut microbiota among individual mice. Nevertheless, core strains like *A. muciniphila* theoretically strengthen intestinal mucosal barrier integrity[32]. This may effectively block the leakage of endotoxins and gut-derived pro-inflammatory factors into the peripheral blood. This barrier protection reduces inflammatory stimulation of the peripheral and central trigeminovascular systems at the source. This is crucial for blocking the cascade of pain sensitization. However, microbiota intervention mechanisms in CM remain highly complex. For example, recent studie highlighted sexual dimorphism in the CM gut microbiota[33]. The abundance of *A. muciniphila* showed an abnormal increasing trend in female

migraine mice. Therefore, sex-specific regulatory networks involving *A. muciniphila* may exist during CM development. The underlying sex hormone-GBA interactions represent an important direction for future research. Furthermore, our current study primarily focused on taxonomic changes of specific key marker bacteria. Future studies should combine metagenomics and untargeted metabolomics. This will comprehensively analyze the systemic effects of KD on the overall microbiome profile and metabolite pool in CM models or patients.

Previous studies confirmed the significant efficacy of KD in CNS diseases such as AD, Parkinson's disease (PD), depression, and epilepsy[34]. KD also demonstrates analgesic properties in various pain models[35–38]. However, its pleiotropic mechanisms in CM remain highly complex. In this study, we primarily focused on the KD-induced remodeling of gut microbiota architecture and function. However, KD is a systemic metabolic intervention. Its biological effects extend far beyond microbiota modulation. KD induces the production of abundant ketone bodies (i.e., β-hydroxybutyrate(BHB), acetoacetate and acetone)[39]. These molecules cross the blood-brain barrier (BBB) and are converted into acetyl-CoA in most organs. This process provides a stable and efficient alternative ATP source for the CNS via the tricarboxylic acid (TCA) cycle and oxidative phosphorylation[40]. Furthermore, growing evidence indicates that ketone bodies are not merely energy substrates. They also act as crucial neural signaling molecules. For instance, BHB directly reduces

abnormal neuronal hyperexcitability in the brain[41]. Additionally, KD activates Sirt3, a core metabolic regulatory node. This activation closely couples mitochondrial integrity maintenance, ketone metabolic homeostasis, and the anti-neuroinflammatory effects of BHB[35]. Moreover, KD-induced microbiota remodeling systematically downregulates intestinal pro-inflammatory Th17 cells at the immunological level[42]. Therefore, the exact mechanisms of KD in alleviating CM are multidimensional. Future research must combine metagenomic and molecular biological approaches for deeper exploration.

We observed that CM was accompanied by significant neuronal sensitization in the PVN. It also triggered abnormal hypersecretion of OT. This is consistent with previous studies. OT is a key neuroendocrine factor. It plays an important role in endogenous pain regulation and stress responses. The NTG-induced sharp increase in OT may reflect a compensatory defense mechanism of the body under severe pain stress. KD downregulated neuronal sensitization and abnormally elevated OT levels in the PVN of CM mice. This phenomenon highly aligns with recent clinical studies on KD intervention in metabolic disorders[43]. Clinical studies show that OT often exhibits a compensatory increase during metabolic imbalances like obesity. A very low-calorie ketogenic diet (VLCKD) intervention helps obese patients achieve rapid weight loss. It subsequently reduces OT levels in their circulatory system. The decline in OT levels reflects local improvement and it also marks the restoration of homeostasis across the entire GBA. Studies have found that OT

effectively inhibits the excessive dopamine response caused by adverse stimuli. It also restricts the body's abnormal stress behavior. Meanwhile, beneficial gut microbes like *A. muciniphila* provide metabolic and neuroprotective support in the GBA. This indicates a close bidirectional interaction mechanism between OT and key gut microbiota[44]. Based on our Spearman’s correlation analysis and the aforementioned literature, we hypothesized that gut microbiota dysbiosis in CM mice weakens the neuroprotective barrier. This dysbiosis includes the sharp decrease in *A. muciniphila* abundance. Consequently, numerous peripheral nociceptive and inflammatory signals invade the CNS. This forces the PVN to produce compensatory OT hypersecretion to cope with severe stress. KD remodels the gut microbiota composition. It re-enriches *A. muciniphila* and other beneficial bacteria to repair the intestinal barrier and anti-inflammatory pathways. With the reduction of ascending neuroinflammation and nociceptive input, the CNS relieves its stress state. This ultimately causes the abnormally elevated OT to decline. This finding clarifies that KD alleviates central sensitization by remodeling gut microbiota composition. It also provides a solid theoretical basis for targeting the "gut microbiota-OT" axis to treat CM.

Conclusion

Our study demonstrates that KD ameliorates hyperalgesia and central sensitization in NTG-induced CM mice. This therapeutic effect may be attributed to the KD-mediated modulation of the gut microbial composition and

552 the reversal of NTG-induced dysbiosis. Furthermore, RNA sequencing
553 analysis revealed that the KD regulates multiple networks associated with
554 neuropeptide signaling in the PVN. We further confirmed that the KD
555 attenuates neuronal hyperexcitability and reduces the aberrant expression of
556 OT within the PVN. In conclusion, our preclinical findings demonstrate that KD
557 effectively mitigates CM in mice. This study provides an experimental basis for
558 exploring KD as a potential dietary intervention in future CM management.
559

560 **Abbreviations**

561 KD: Ketogenic diet; CM: Chronic migraine; GBA: Gut-brain axis; NTG:
562 Nitroglycerin; TNC: Trigeminal nucleus caudalis; CGRP: Calcitonin
563 gene-related peptide; PVN: Paraventricular nucleus of the hypothalamus; GBD:
564 Global Burden of Disease Study; FMT: Fecal microbiota transplantation;
565 SCFAs: Short-chain fatty acids; SP: Sodium propionate; SB: Sodium butyrate;
566 CNS: Central nervous system; PCA: Principal component analysis; PFA:
567 Polyformaldehyde; PBS: Phosphate-buffered saline; DAPI:
568 4′,6-diamidino-2-phenylindole; OTUs: Operational taxonomic units; PCoA:
569 Principal coordinate analysis; ANOSIM: Analysis of similarities; PTS:
570 Phosphotransferase system; GSEA: Gene set enrichment analysis; KEGG:
571 Kyoto Encyclopedia of Genes and Genomes; GO: Gene Ontology; OT:
572 Oxytocin; DALY: Disability-Adjusted Life Years; AD: Alzheimer's disease; PD:
573 Parkinson's disease; TCA: Tricarboxylic Acid; BHB: β-hydroxybutyrate;

VLCKD: Very Low-Calorie Ketogenic Diet; BBB: Blood-brain barrier.

Acknowledgements

We are sincerely grateful to all the staff of Lanzhou Veterinary Research Institute.

Authors' contributions

JLZ and ZCZ contributed with the conception and design of the work. JLZ, LW, LMF, JFL, ZHK, YBW, CG, GS and YGW contributed to the acquisition, analysis, and interpretation of data. JLZ drafted the manuscript, and all authors critically reviewed the manuscript before submission.

Funding

This study was supported by the Academician Workstation of The Second Hospital & Clinical Medical School, Lanzhou University Fund; Gansu Provincial Health Industry Science and Technology Innovation Project (GSWSQNPY2025-03); National Natural Science Foundation of China, Youth Science Fund Project (82602845); Cuiying Scientific and Technological Innovation Program of The Second Hospital & Clinical Medical School, Lanzhou University (CY2025-MS-A08);

Data availability

All data generated or analyzed during this study are included in this article. Further inquiries can be directed to the corresponding author upon reasonable request.

Declarations

Ethics approval and Consent to Participate

The animal study was reviewed and approved by the Animal Ethics Committee of Lanzhou University Second Hospital (D2025-900)

Consent for publication

Not applicable.

Competing interests

The authors declare that they have no competing interests.

Author details

[1] Department of Neurology, The Second Hospital of Lanzhou University, Gate, No. 82 Linxia Road, Chengguan District, Lanzhou 730000, China.

[2] Institute of Genetics, School of Basic Medical Sciences, Lanzhou University, Lanzhou, Gansu, China.

[3] Headache Center, Department of Neurology, Beijing Tiantan Hospital, Capital Medical University, No.119 South Fourth Ring West Road, Fengtai District, Beijing 100070, China.

References

1. GBD 2021 Nervous System Disorders Collaborators (2024) Global, regional, and national burden of disorders affecting the nervous system, 1990-2021: a systematic analysis for the Global Burden of Disease Study 2021. Lancet Neurol 23:344–381.

2. Dodick DW (2018) Migraine. Lancet 391:1315–1330.

618 3. Cámara-Lemarroy CR, Rodriguez-Gutierrez R, Monreal-Robles R,
619 Marfil-Rivera A (2016) Gastrointestinal disorders associated with migraine:
620 A comprehensive review. World J Gastroenterol 22:8149–8160.

621 4. Hindiyeh N, Aurora SK (2015) What the Gut Can Teach Us About
622 Migraine. Curr Pain Headache Rep 19:33.

623 5. van Hemert S, Breedveld AC, Rovers JMP, et al (2014) Migraine
624 associated with gastrointestinal disorders: review of the literature and
625 clinical implications. Front Neurol 5:241.

626 6. Tang Y, Liu S, Shu H, et al (2020) Gut Microbiota Dysbiosis Enhances
627 Migraine-Like Pain Via TNFα Upregulation. Mol Neurobiol 57:461–468.

628 7. Kang L, Tang W, Zhang Y, et al (2022) The gut microbiome modulates
629 nitroglycerin-induced migraine-related hyperalgesia in mice. Cephalalgia
630 42:490–499.

631 8. Lanza M, Filippone A, Ardizzone A, et al (2021) SCFA Treatment
632 Alleviates Pathological Signs of Migraine and Related Intestinal
633 Alterations in a Mouse Model of NTG-Induced Migraine. Cells 10:2756.

634 9. Martin CR, Osadchiy V, Kalani A, Mayer EA (2018) The
635 Brain-Gut-Microbiome Axis. Cell Mol Gastroenterol Hepatol 6:133–148.

636 10. Loh JS, Mak WQ, Tan LKS, et al (2024) Microbiota-gut-brain axis and its

637 therapeutic applications in neurodegenerative diseases. Signal Transduct
638 Target Ther 9:37.

639 11. Wang D, Liu X, Shi S, et al (2023) Gut microbiota and metabolite
640 variations in a migraine mouse model. Front Cell Infect Microbiol
641 13:1322059.

642 12. Chen C, He J, Ma Z, et al (2026) Sex differences in behaviors, neuronal
643 activation, and gut-microbiota-metabolic axis in a repeated
644 nitroglycerin-induced chronic migraine model. J Headache Pain 27:139.

645 13. Miao S, Tang W, Li H, et al (2022) Repeated inflammatory dural
646 stimulation-induced cephalic allodynia causes alteration of gut microbial
647 composition in rats. J Headache Pain 23:71.

648 14. Seng EK, Martin PR, Houle TT (2022) Lifestyle factors and migraine.
649 Lancet Neurol 21:911–921.

650 15. Lovati C, d'Alessandro CM, Ventura SD, et al (2022) Ketogenic diet in
651 refractory migraine: possible efficacy and role of ketone bodies-a pilot
652 experience. Neurol Sci 43:6479–6485.

653 16. Di Lorenzo C, Pinto A, Ienca R, et al (2019) A Randomized Double-Blind,
654 Cross-Over Trial of very Low-Calorie Diet in Overweight Migraine Patients:
655 A Possible Role for Ketones? Nutrients 11:1742.

656 17. Bough KJ, Wetherington J, Hassel B, et al (2006) Mitochondrial
657 biogenesis in the anticonvulsant mechanism of the ketogenic diet. Ann
658 Neurol 60:223–235.

659 18. Liu C, Zhang N, Zhang R, et al (2020) Cuprizone-Induced Demyelination
660 in Mouse Hippocampus Is Alleviated by Ketogenic Diet. J Agric Food
661 Chem 68:11215–11228.

662 19. de Almeida Rabello Oliveira M, da Rocha Ataíde T, de Oliveira SL, et al
663 (2008) Effects of short-term and long-term treatment with medium- and
664 long-chain triglycerides ketogenic diet on cortical spreading depression in
665 young rats. Neurosci Lett 434:66–70.

666 20. Akerman S, Karsan N, Bose P, et al (2019) Nitroglycerine triggers
667 triptan-responsive cranial allodynia and trigeminal neuronal
668 hypersensitivity. Brain 142:103–119.

669 21. Christensen SL, Hansen RB, Storm MA, et al (2020) Von Frey testing
670 revisited: Provision of an online algorithm for improved accuracy of 50%
671 thresholds. Eur J Pain 24:783–790.

672 22. Papetti L, Del Chierico F, Frattale I, et al (2024) Pediatric migraine is
673 characterized by traits of ecological and metabolic dysbiosis and
674 inflammation. J Headache Pain 25:171.

675 23. Cani PD, Depommier C, Derrien M, et al (2022) Akkermansia muciniphila:

paradigm for next-generation beneficial microorganisms. Nat Rev Gastroenterol Hepatol 19:625–637.

24. Olson CA, Vuong HE, Yano JM, et al (2018) The Gut Microbiota Mediates the Anti-Seizure Effects of the Ketogenic Diet. Cell 173:1728-1741.e13.

25. Ou Z, Deng L, Lu Z, et al (2020) Protective effects of Akkermansia muciniphila on cognitive deficits and amyloid pathology in a mouse model of Alzheimer's disease. Nutr Diabetes 10:12.

26. Miao S, Tang W, Li H, et al (2022) Repeated inflammatory dural stimulation-induced cephalic allodynia causes alteration of gut microbial composition in rats. J Headache Pain 23:71.

27. Suthivanich P, Vongseenin S, Auvichayapat V, et al (2025) Probiotic modulation of central and peripheral sensitization in a migraine model via the gut-brain-trigeminal axis. Sci Rep 15:41103.

28. Park JC, Sim M-A, Lee C, et al (2025) Gut microbiota and brain-resident CD4+ T cells shape behavioral outcomes in autism spectrum disorder. Nat Commun 16:6422.

29. Mazzoli A, Spagnuolo MS, De Palma F, et al (2024) Limosilactobacillus reuteri DSM 17938 relieves inflammation, endoplasmic reticulum stress, and autophagy in hippocampus of western diet-fed rats by modulation of systemic inflammation. Biofactors 50:1236–1250.

30. Li N, Peng X, Xiong W, et al (2026) The gut microbiota-brain axis in Alzheimer's disease model mice. Physiol Behav 304:115178.

31. Chen M-L, He Y, Dong X-H, et al (2025) Ketogenic diet inhibits glioma progression by promoting gut microbiota-derived butyrate production. Cancer Cell 43:2119-2135.e10.

32. Paone P, Cani PD (2020) Mucus barrier, mucins and gut microbiota: the expected slimy partners? Gut 69:2232–2243.

33. Chen C, He J, Ma Z, et al (2026) Sex differences in behaviors, neuronal activation, and gut-microbiota-metabolic axis in a repeated nitroglycerin-induced chronic migraine model. J Headache Pain 27:139.

34. Pietrzak D, Kasperek K, Rękawek P, Piątkowska-Chmiel I (2022) The Therapeutic Role of Ketogenic Diet in Neurological Disorders. Nutrients 14:1952.

35. Deng M, Fang Y, Chu Y, et al (2025) SIRT3 is required for the protective function of ketogenic diet on neural inflammation and neuropathic pain. Int J Biol Sci 21:3011–3029.

36. Enders J, Swanson MT, Ryals J, Wright DE (2022) A ketogenic diet reduces mechanical allodynia and improves epidermal innervation in diabetic mice. Pain 163:682–689.

715 37. Enders JD, Thomas S, Swanson MT, et al (2022) Ketogenic diet prevents
716 methylglyoxal-evoked nociception by scavenging methylglyoxal. Pain
717 163:e1207–e1216.

718 38. Crawford J, Liu S, Tao R, et al (2024) The ketogenic diet mitigates
719 opioid-induced hyperalgesia by restoring short-chain fatty
720 acids-producing bacteria in the gut. Pain 165:e106–e114.

721 39. Laffel L (1999) Ketone bodies: a review of physiology, pathophysiology
722 and application of monitoring to diabetes. Diabetes Metab Res Rev
723 15:412–426.

724 40. Manninen AH (2004) Metabolic effects of the very-low-carbohydrate diets:
725 misunderstood “villains” of human metabolism. J Int Soc Sports Nutr 1:7–
726 11.

727 41. Lutas A, Yellen G (2013) The ketogenic diet: metabolic influences on
728 brain excitability and epilepsy. Trends Neurosci 36:32–40.

729 42. Ang QY, Alexander M, Newman JC, et al (2020) Ketogenic Diets Alter the
730 Gut Microbiome Resulting in Decreased Intestinal Th17 Cells. Cell
731 181:1263-1275.e16.

732 43. Gangitano E, Rossetti R, Tozzi R, et al (2026) Oxytocin, Weight Loss and
733 Ketosis in Response to a Very-Low-Calorie Ketogenic Diet: An
734 Exploratory Study. Nutrients 18:485.

44. Coccurello R (2025) Disrupting the Gut-Brain Axis: How Artificial Sweeteners Rewire Microbiota and Reward Pathways. Int J Mol Sci 26:10220.

Graphical Abstract: All schematic illustrations were generated using Biorender.

Figure 1. Effects of KD on NTG-induced CM-like behavioral hypersensitivity in mice. (A) Macronutrient composition of the SD and KD, showing the percentage of calories derived from carbohydrate, fat, and protein. (B) Changes in blood ketone levels (mg/dL) in mice measured at days 0, 10, 20, and 30 across experimental groups (VEH, NTG, and KD-NTG). (C) Time course of body weight changes (g) measured at the indicated time points (0D, 10D, 20D, and 30D). (D) Schematic timeline of the experimental protocol. (E) Periorbital mechanical withdrawal thresholds (g) evaluated with von Frey filaments. (F) Hind paw mechanical withdrawal thresholds (g). (G) Hind paw thermal withdrawal latency (s) assessed by hot plate test (55°C). Data are presented as mean±SEM (n = 10 mice per group). #p < 0.05, ##p < 0.01, ###p < 0.001, ####p < 0.0001, NTG group compared with the VEH group, *p < 0.05, **p < 0.01, ***p < 0.001, ****p < 0.001, KD-NTG group compared with the NTG group. Abbreviations: VEH, Vehicle; NTG, Nitroglycerin; KD, Ketogenic diet; SD, Standard diet; CM, Chronic migraine.

Figure 2. KD suppresses NTG-induced neuronal sensitization and microglial activation in the TNC. (A) Representative immunofluorescence staining views showing CGRP immunoreactivity in the TNC across VEH, NTG, KD-NTG groups. (B) Representative immunofluorescence staining views showing c-Fos positive cells within the TNC region. (C) Quantitative analysis of the relative fluorescence intensity of CGRP in the TNC. (D) Quantitative analysis of the number of c-Fos positive cells per slice in the TNC. (E) Representative immunofluorescence staining for the microglial marker Iba-1 in the TNC and high-magnification images depicting single-microglia morphology. (F-I) Quantitative morphological analysis of microglial activation: (F) Number of Iba-1 positive cells per slice in the TNC; (G) Microglial soma size; (H) Total process length per cell; (I) Number of process endpoints per cell. Data are presented as mean±SEM (n = 4 mice per group). *p < 0.05, **p < 0.01, ***p < 0.001, ****p < 0.001, KD-NTG group compared with the NTG group. Abbreviations: VEH, Vehicle; NTG, Nitroglycerin; KD, Ketogenic diet; TNC, Trigeminal nucleus caudalis; CGRP, Calcitonin gene-related peptide; Iba1, Ionized calcium-binding adapter molecule 1.

Figure 3. KD remodels gut microbiota composition and diversity in NTG-induced CM mice. (A) UpSet plot illustrating the shared and unique operational taxonomic units among the VEH, NTG, and KD-NTG groups. (B) PCoA score plot based on Bray-Curtis dissimilarity, showing distinct clustering

of gut microbial communities among groups. (C) ANOSIM box plot based on Bray-Curtis distances demonstrating microbial community differences between and within groups. (D) Stacked bar plot showing the relative abundance of gut microbiota at the phylum level across individual mice in each group. (E) Hierarchical clustering heatmap of differentially abundant taxa at the genus level across samples. (F) Extended error bar plot showing significantly different taxa among groups. (G-J) Box plots showing the sequence proportions of key altered taxa: (G) genus *Ligilactobacillus*; (H) genus *Dubosiella*; (I) genus *Adlercreutzia*; (J) genus *Faecalibaculum*. Data are presented as mean ± SEM (n = 6 mice per group). *p < 0.05, **p < 0.01,***p < 0.001, KD-NTG group compared with the NTG group. Abbreviations: VEH, Vehicle; NTG, Nitroglycerin; KD, Ketogenic diet; PCoA, Principal coordinates analysis; ANOSIM, Analysis of similarities.

Figure 4. Correlation analysis of gut microbiota and functional pathway prediction. (A) LEfSe bar plot identifying the biomarker taxa with significantly differential abundance among the VEH, NTG, and KD-NTG groups, represented by their LDA scores. (B) Spearman's correlation heatmap of the differentially abundant gut microbiota at the genus level. (C) Comparison of predicted KEGG Level 1 functional pathways using PICRUSt between the NTG and KD-NTG groups. (D) Heatmap depicting the relative abundance of predicted functional pathways across individual samples. (n = 6 mice per

group). *p < 0.05, **p < 0.01, ***p < 0.001, KD-NTG group compared with the NTG group. Abbreviations: VEH, Vehicle; NTG, Nitroglycerin; KD, Ketogenic diet; LEfSe, Linear discriminant analysis effect size; LDA, Linear discriminant analysis; KEGG, Kyoto encyclopedia of genes and genomes.

Figure 5. Retrograde transsynaptic viral tracing from the ascending colon and neuronal activation in the PVN region. (A) Schematic diagram of the experimental tracing protocol: PRV-CAG-mRFP was injected into the ascending colon to trace the retrograde neural circuits projecting to the brain. (B) Representative immunofluorescence images showing the expression and co-localization of the retrograde transsynaptic tracer PRV-CAG-mRFP (red) and the neuronal activation marker c-Fos (green) in the brain. (C) Pie chart illustrating the percentage of PRV-CAG-mRFP/c-Fos double-positive neurons (35.8%). (n = 4 mice per group). Abbreviations: PVN, Paraventricular hypothalamic nucleus.

Figure 6. Transcriptomic analysis reveals the modulatory effects of KD on gene expression in NTG-induced mice. (A) PCA: score plot showing the overall transcriptional variations among the VEH, NTG, and KD-NTG groups. (B) Hierarchical clustering heatmap of directionally counter-regulated genes, illustrating their relative expression patterns across the three groups. (C) GSEA of GO BP comparing the KD-NTG group with the NTG group. (D)

Bubble plot showing the GO BP over-representation analysis of all counter-regulated genes. (E) Bubble plot showing the GO MF over-representation analysis of all counter-regulated genes. (n = 4 mice per group). Abbreviations: VEH, Vehicle; NTG, Nitroglycerin; KD, Ketogenic diet; PCA, Principal component analysis; GSEA, Gene set enrichment analysis; GO, Gene ontology; BP, Biological process; MF, Molecular function.

Figure 7. KD modulates c-Fos and OT expression in the PVN region of NTG-induced CM mice. (A) Representative immunofluorescence images showing c-Fos expression in the PVN region across the VEH, NTG, and KD-NTG groups. (B) Representative immunofluorescence images showing OT immunoreactivity in the PVN region across the experimental groups. (C) Quantitative analysis of the number of c-Fos-positive cells per slice in the PVN region. (D) Quantitative analysis of serum OT concentration (pg/ml) across the groups. (E) Quantitative analysis of the number of OT-positive cells per slice in the PVN region. Data are presented as mean±SEM (n = 4 mice per group). *p < 0.05, **p < 0.01, ***p < 0.001, ****p < 0.001, KD-NTG group compared with the NTG group. Abbreviations: VEH, Vehicle; NTG, Nitroglycerin; KD, Ketogenic diet; PVN, Paraventricular hypothalamic nucleus; OT, Oxytocin.

Figure 8. KD modulates gut microbiota composition and correlates with neurobiological indicators in CM mice. (A) Heatmap showing the relative

abundance of gut microbiota at the species level across the VEH, NTG, and KD-NTG groups. (B) Bar graph illustrating the relative abundance of *Akkermansia muciniphila* in the VEH, NTG, and KD-NTG groups. (C) Spearman correlation heatmap of interactions among gut microbiota at the species level. (D) Spearman correlation heatmap between differential gut microbiota and neurobiological indicators (microglial branches, microglial endpoints, iba-1+, microglial soma size, c-fos+, OT). Data are presented as mean±SEM (n = 6 mice per group). *p < 0.05; **p < 0.01; ***p < 0.001. Abbreviations: VEH, Vehicle; NTG, Nitroglycerin; KD, Ketogenic diet; CM, Chronic migraine; OT, Oxytocin.

Supplementary Figure 1. Alpha diversity analysis of the gut microbiota. (A-D) Box plots showing the evaluation of alpha diversity indices in fecal samples across the experimental groups (VEH, NTG, and KD-NTG): (A) Coverage index; (B) Shannon index; (C) ACE index; (D) Simpson index. Data are presented as mean ± SEM (n = 6 mice per group). *p < 0.05, **p < 0.01, ***p < 0.001, ****p < 0.001, KD-NTG group compared with the NTG group. Abbreviations: VEH, Vehicle; NTG, Nitroglycerin; KD, Ketogenic diet.

Supplementary Figure 2. Compositional differences and analysis of gut microbiota at the family level. (A) Hierarchical clustering heatmap of

differentially abundant taxa at the family level across the VEH, NTG, and KD-NTG groups. (B) Bar plot showing the mean proportions (%) of significantly different bacterial families among the groups. (C-F) Box plots showing the sequence proportions of key altered microbial taxa among the VEH, NTG, and KD-NTG groups: (C) family Lachnospiraceae; (D) family Desulfovibrionaceae; (E) family Oscillospiraceae; (F) family Akkermansiaceae. Data are presented as mean ± SEM (n = 6 mice per group). *p < 0.05, **p < 0.01, ***p < 0.001, ****p < 0.001, KD-NTG group compared with the NTG group. Abbreviations: VEH, Vehicle; NTG, Nitroglycerin; KD, Ketogenic diet.

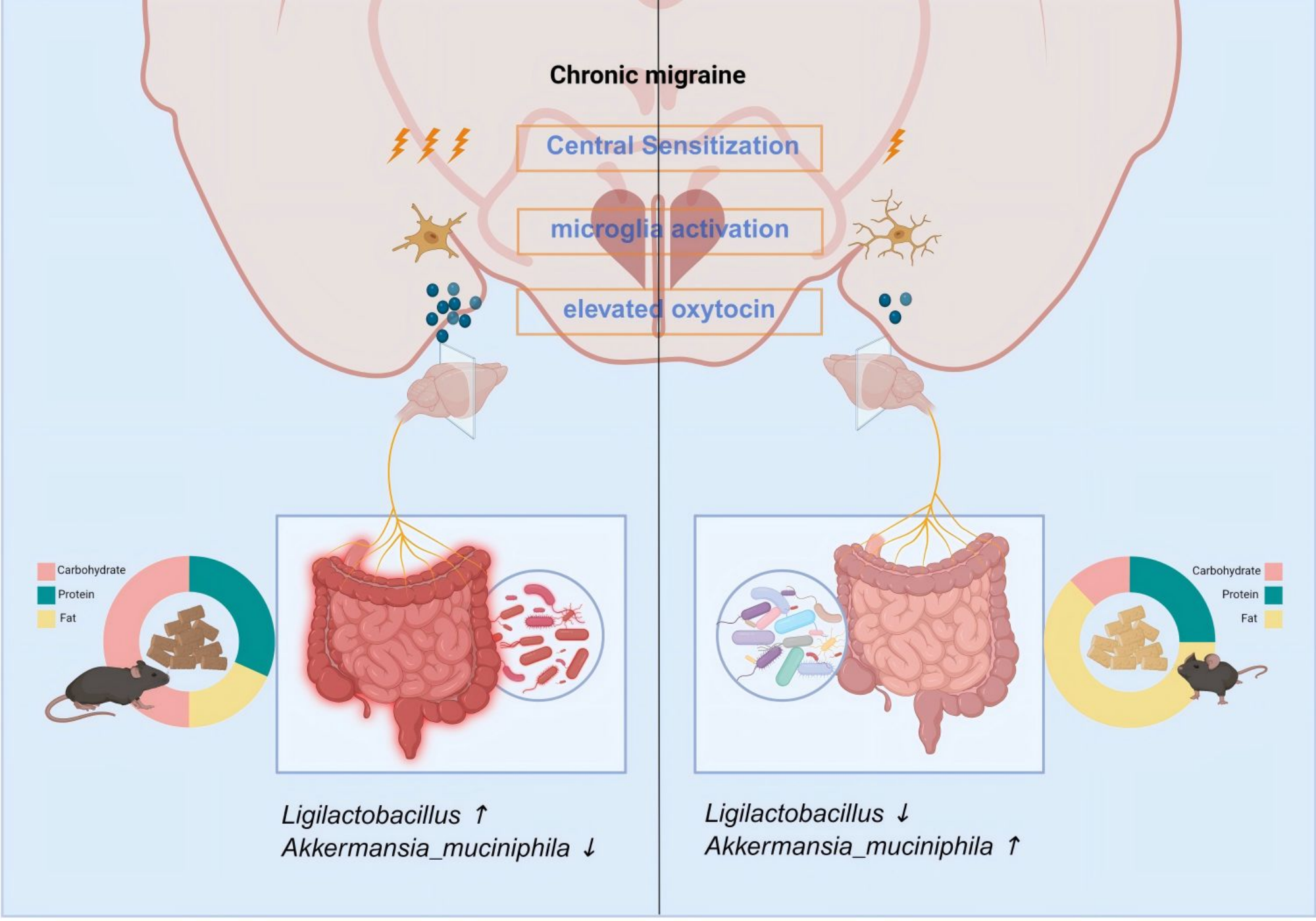
Chronic migraine
Central Sensitization
microglia activation
elevated oxytocin
Carbohydrate
Protein
Fat
Ligilactobacillus ↑
Akkermansia_muciniphila ↓
Carbohydrate
Protein
Fat
Ligilactobacillus ↓
Akkermansia_muciniphila ↑

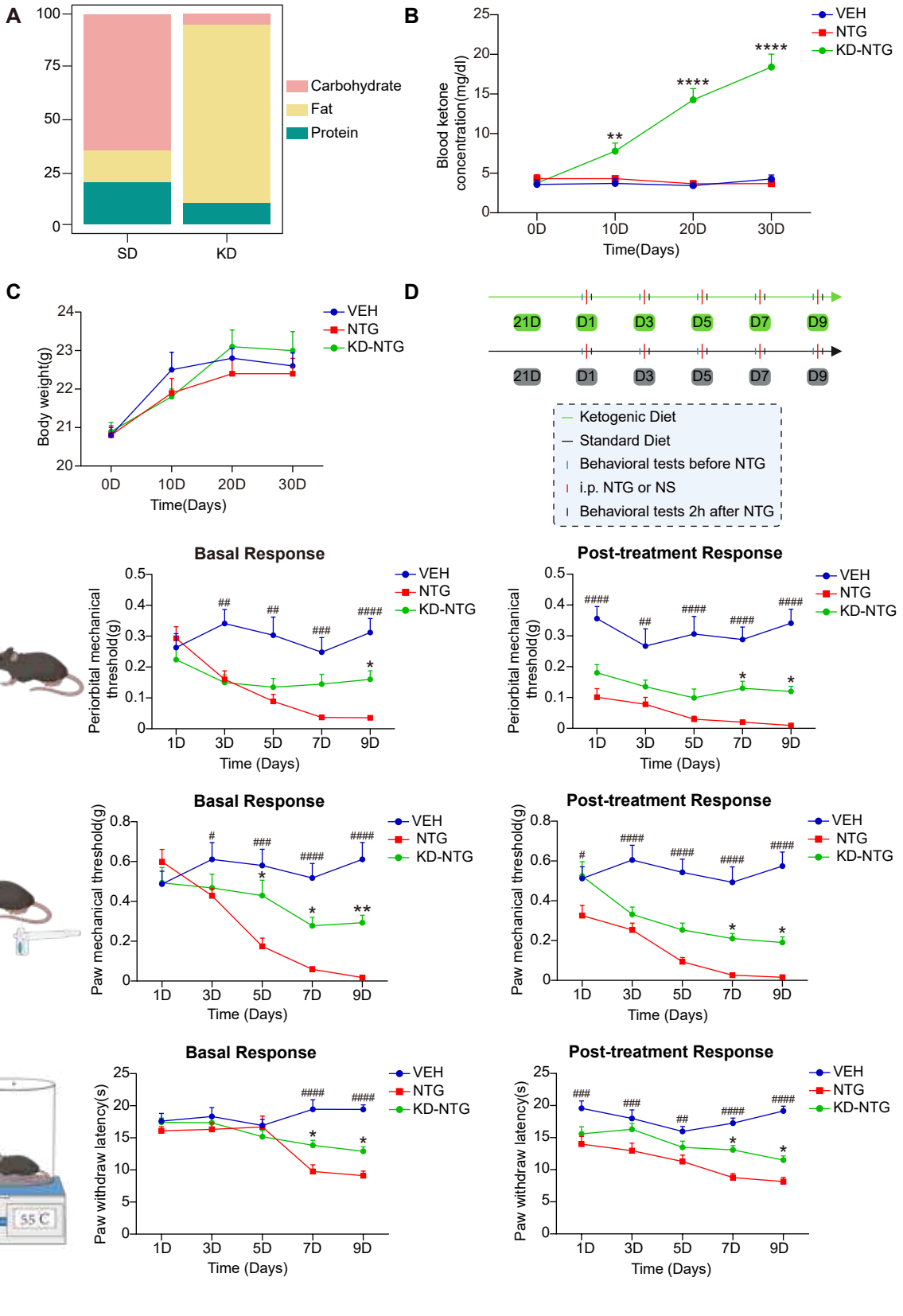
A
100
75
50
25
0
SD
KD
Carbohydrate
Fat
Protein
B
Blood ketone concentration(mg/dl)
25
20
15
10
5
0
0D
10D
20D
30D
Time(Days)
**
****
****
VEH
NTG
KD-NTG
C
Body weight(g)
24
23
22
21
20
0D
10D
20D
30D
Time(Days)
VEH
NTG
KD-NTG
D
21D
D1
D3
D5
D7
D9
Ketogenic Diet
Standard Diet
Behavioral tests before NTG
i.p. NTG or NS
Behavioral tests 2h after NTG
E
Basal Response
Post-treatment Response
Periorbital mechanical threshold(g)
0.5
0.4
0.3
0.2
0.1
0
1D
3D
5D
7D
9D
Time (Days)
VEH
NTG
KD-NTG
F
Basal Response
Post-treatment Response
Paw mechanical threshold(g)
0.8
0.6
0.4
0.2
0
Time (Days)
G
Basal Response
Post-treatment Response
Paw withdraw latency(s)
25
20
15
10
5
0
55 C
Time (Days)

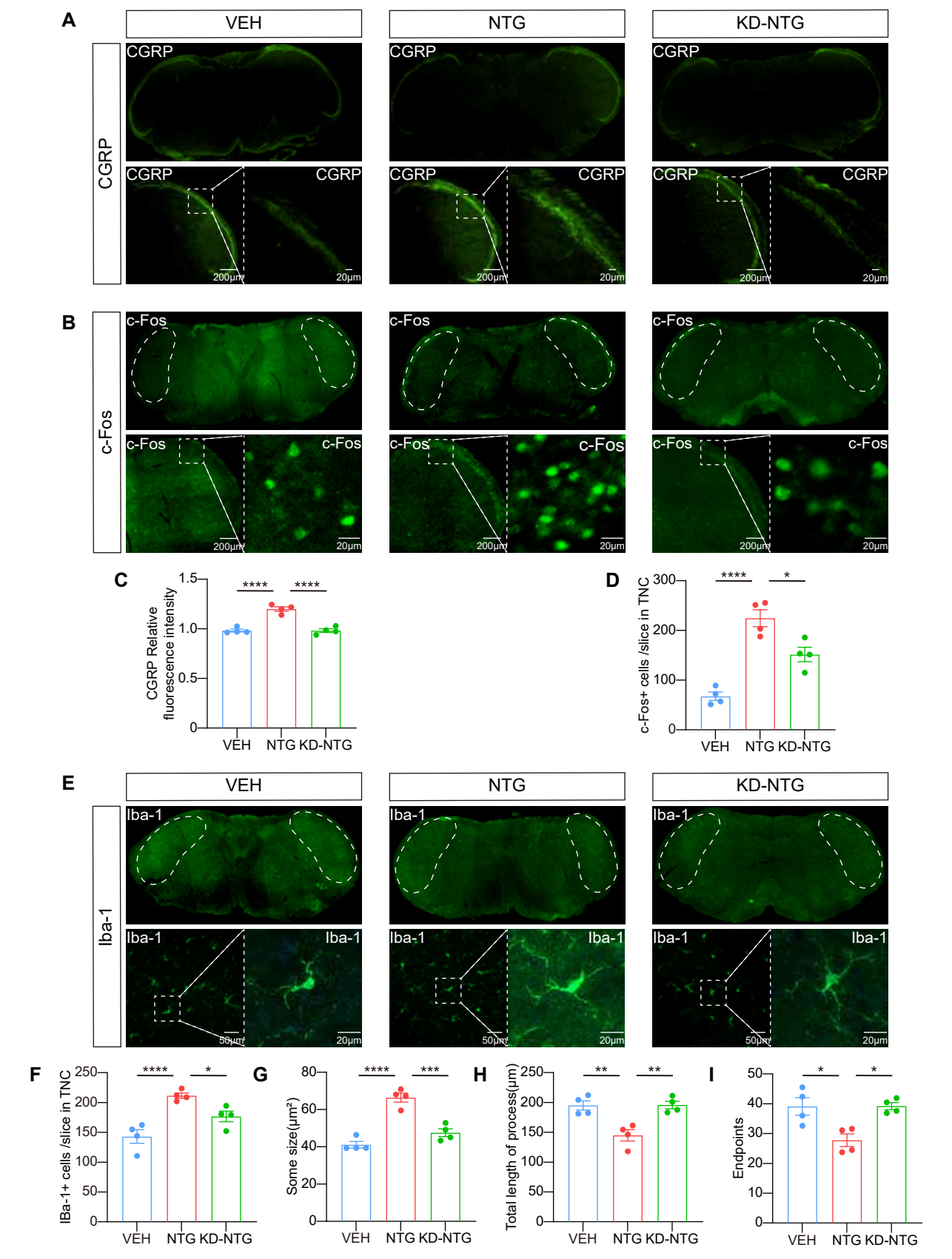
A
VEH
NTG
KD-NTG
CGRP
CGRP
CGRP
CGRP
CGRP
CGRP
CGRP
CGRP
CGRP
200μm
20μm
B
c-Fos
c-Fos
c-Fos
c-Fos
c-Fos
c-Fos
c-Fos
c-Fos
c-Fos
200μm
20μm
C
CGRP Relative fluorescence intensity
1.5
1.0
0.5
0
****
****
VEH
NTG
KD-NTG
D
c-Fos+ cells /slice in TNC
300
200
100
0
****
*
VEH
NTG
KD-NTG
E
VEH
NTG
KD-NTG
Iba-1
Iba-1
Iba-1
Iba-1
Iba-1
Iba-1
Iba-1
Iba-1
Iba-1
50μm
20μm
F
IBa-1+ cells /slice in TNC
250
200
150
100
50
0
****
*
VEH
NTG
KD-NTG
G
Some size(μm²)
80
60
40
20
0
****
***
VEH
NTG
KD-NTG
H
Total length of process(μm)
250
200
150
100
50
0
**
**
VEH
NTG
KD-NTG
I
Endpoints
50
40
30
20
10
0
*
*
VEH
NTG
KD-NTG

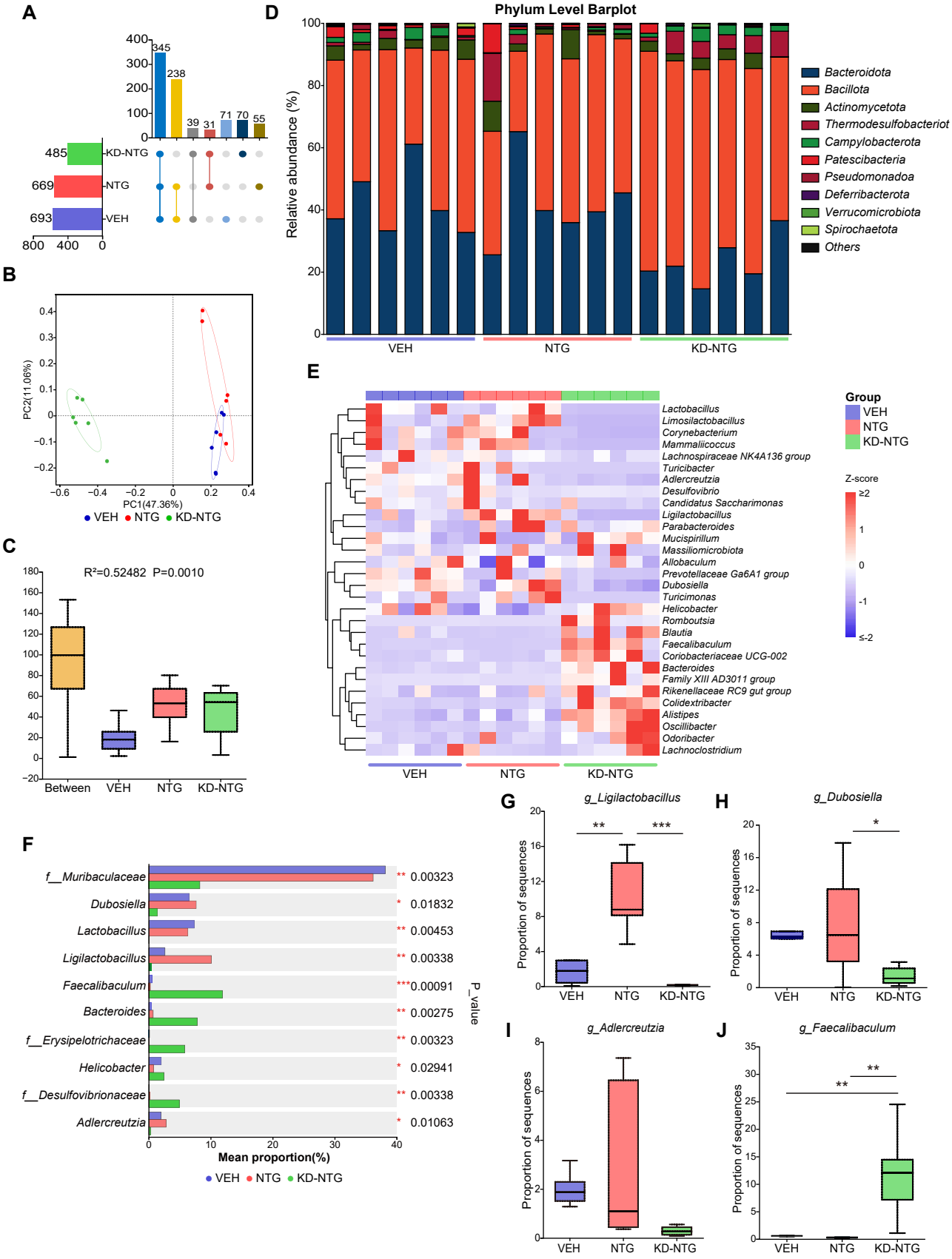
A
345
238
39
31
71
70
55
485
669
693
KD-NTG
NTG
VEH
800 400 0
B
PC2(11.06%)
PC1(47.36%)
VEH NTG KD-NTG
C
R²=0.52482 P=0.0010
Between VEH NTG KD-NTG
D
Phylum Level Barplot
Relative abundance (%)
Bacteroidota
Bacillota
Actinomycetota
Thermodesulfobacteriot
Campylobacterota
Patescibacteria
Pseudomonadoa
Deferribacterota
Verrucomicrobiota
Spirochaetota
Others
VEH NTG KD-NTG
E
Group
VEH
NTG
KD-NTG
Z-score
≥2
1
0
-1
≤-2
Lactobacillus
Limosilactobacillus
Corynebacterium
Mammaliicoccus
Lachnospiraceae NK4A136 group
Turicibacter
Adlercreutzia
Desulfovibrio
Candidatus Saccharimonas
Ligilactobacillus
Parabacteroides
Mucispirillum
Massiliomicrobiota
Allobaculum
Prevotellaceae Ga6A1 group
Dubosiella
Turicimonas
Helicobacter
Romboutsia
Blautia
Faecalibaculum
Coriobacteriaceae UCG-002
Bacteroides
Family XIII AD3011 group
Rikenellaceae RC9 gut group
Colidextribacter
Alistipes
Oscillibacter
Odoribacter
Lachnoclostridium
VEH NTG KD-NTG
F
f__Muribaculaceae ** 0.00323
Dubosiella * 0.01832
Lactobacillus ** 0.00453
Ligilactobacillus ** 0.00338
Faecalibaculum *** 0.00091
Bacteroides ** 0.00275
f__Erysipelotrichaceae ** 0.00323
Helicobacter * 0.02941
f__Desulfovibrionaceae ** 0.00338
Adlercreutzia * 0.01063
P_value
Mean proportion(%)
VEH NTG KD-NTG
G
g_Ligilactobacillus
Proportion of sequences
VEH NTG KD-NTG
H
g_Dubosiella
Proportion of sequences
VEH NTG KD-NTG
I
g_Adlercreutzia
Proportion of sequences
VEH NTG KD-NTG
J
g_Faecalibaculum
Proportion of sequences
VEH NTG KD-NTG

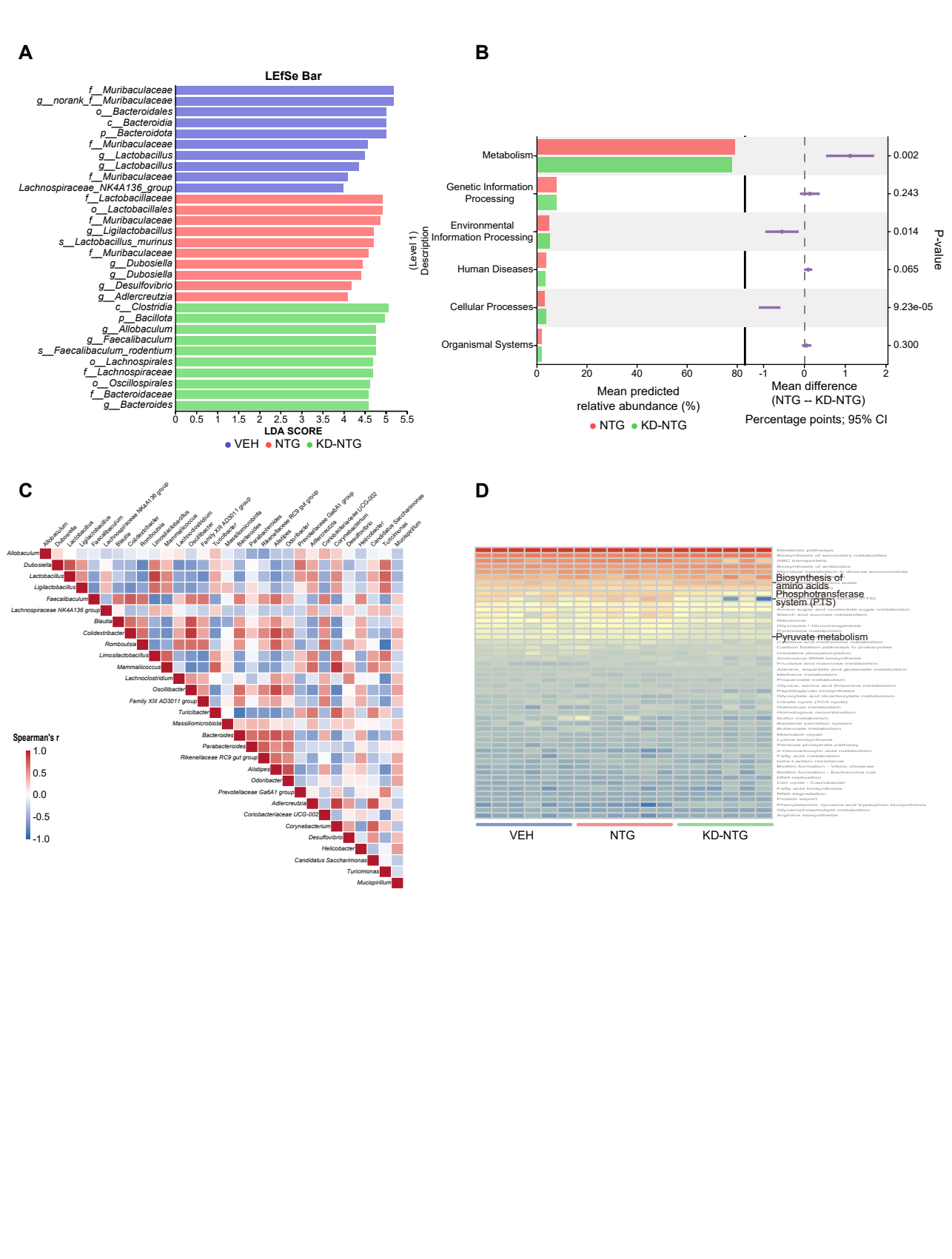
A
LEfSe Bar
f__Muribaculaceae
g__norank_f__Muribaculaceae
o__Bacteroidales
c__Bacteroidia
p__Bacteroidota
f__Muribaculaceae
g__Lactobacillus
g__Lactobacillus
f__Muribaculaceae
Lachnospiraceae_NK4A136_group
f__Lactobacillaceae
o__Lactobacillales
f__Muribaculaceae
g__Ligilactobacillus
s__Lactobacillus_murinus
f__Muribaculaceae
g__Dubosiella
g__Dubosiella
g__Desulfovibrio
g__Adlercreutzia
c__Clostridia
p__Bacillota
g__Allobaculum
g__Faecalibaculum
s__Faecalibaculum_rodentium
o__Lachnospirales
f__Lachnospiraceae
o__Oscillospirales
f__Bacteroidaceae
g__Bacteroides
0 0.5 1 1.5 2 2.5 3 3.5 4 4.5 5 5.5
LDA SCORE
VEH NTG KD-NTG
B
Metabolism
Genetic Information Processing
Environmental Information Processing
Human Diseases
Cellular Processes
Organismal Systems
(Level 1) Description
0.002
0.243
0.014
0.065
9.23e-05
0.300
P-value
0 20 40 60 80
Mean predicted relative abundance (%)
-1 0 1 2
Mean difference (NTG -- KD-NTG)
NTG KD-NTG
Percentage points; 95% CI
C
Allobaculum
Dubosiella
Lactobacillus
Ligilactobacillus
Faecalibaculum
Lachnospiraceae NK4A136 group
Blautia
Colidextribacter
Romboutsia
Limosilactobacillus
Mammaliicoccus
Lachnoclostridium
Oscillibacter
Family XIII AD3011 group
Turicibacter
Massiliomicrobiota
Bacteroides
Parabacteroides
Rikenellaceae RC9 gut group
Alistipes
Odoribacter
Prevotellaceae Ga6A1 group
Adlercreutzia
Coriobacteriaceae UCG-002
Corynebacterium
Desulfovibrio
Helicobacter
Candidatus Saccharimonas
Turicimonas
Mucispirillum
Spearman's r
1.0
0.5
0.0
-0.5
-1.0
D
Biosynthesis of amino acids
Phosphotransferase system (PTS)
Pyruvate metabolism
VEH NTG KD-NTG

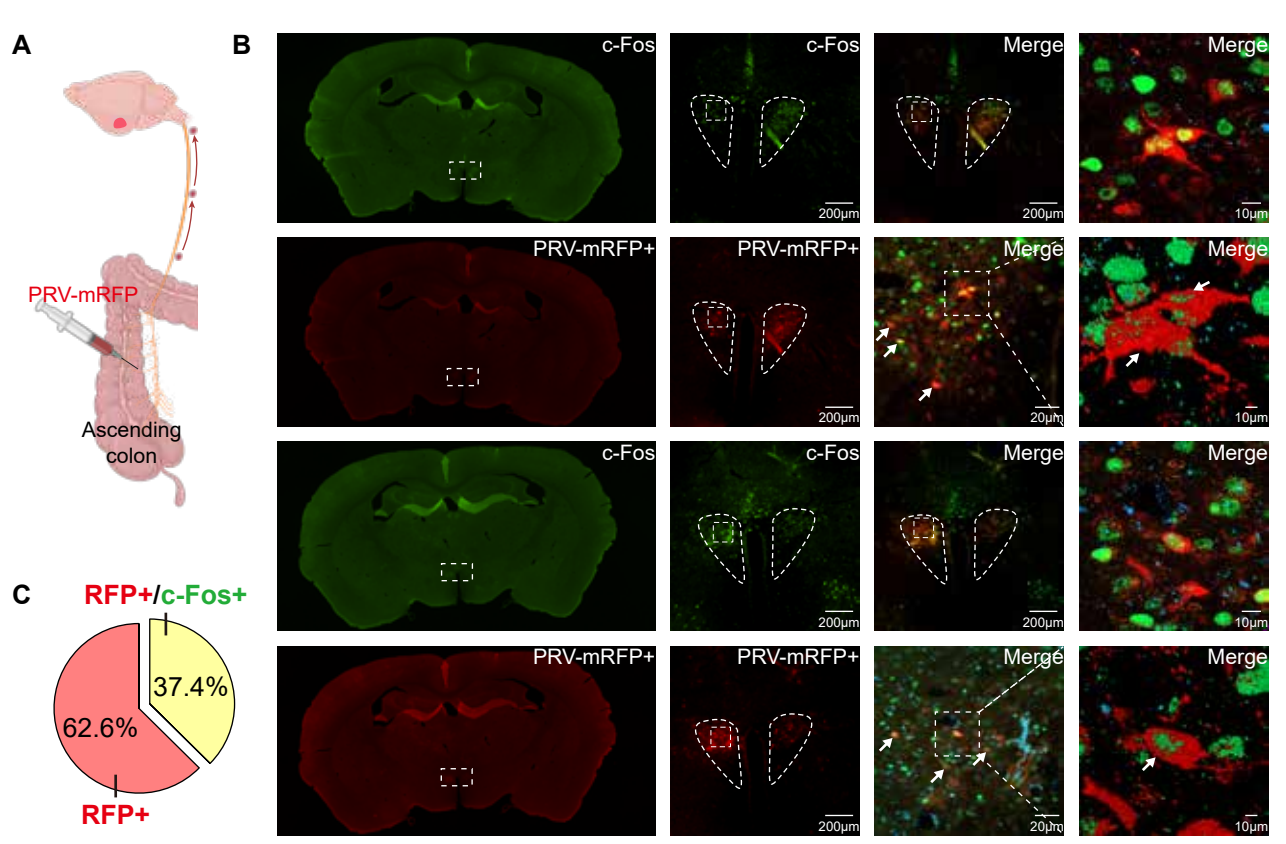
A
PRV-mRFP
Ascending colon
B
c-Fos
c-Fos
Merge
Merge
PRV-mRFP+
PRV-mRFP+
Merge
Merge
c-Fos
c-Fos
Merge
Merge
PRV-mRFP+
PRV-mRFP+
Merge
Merge
200μm
20μm
10μm
C
RFP+/c-Fos+
37.4%
62.6%
RFP+

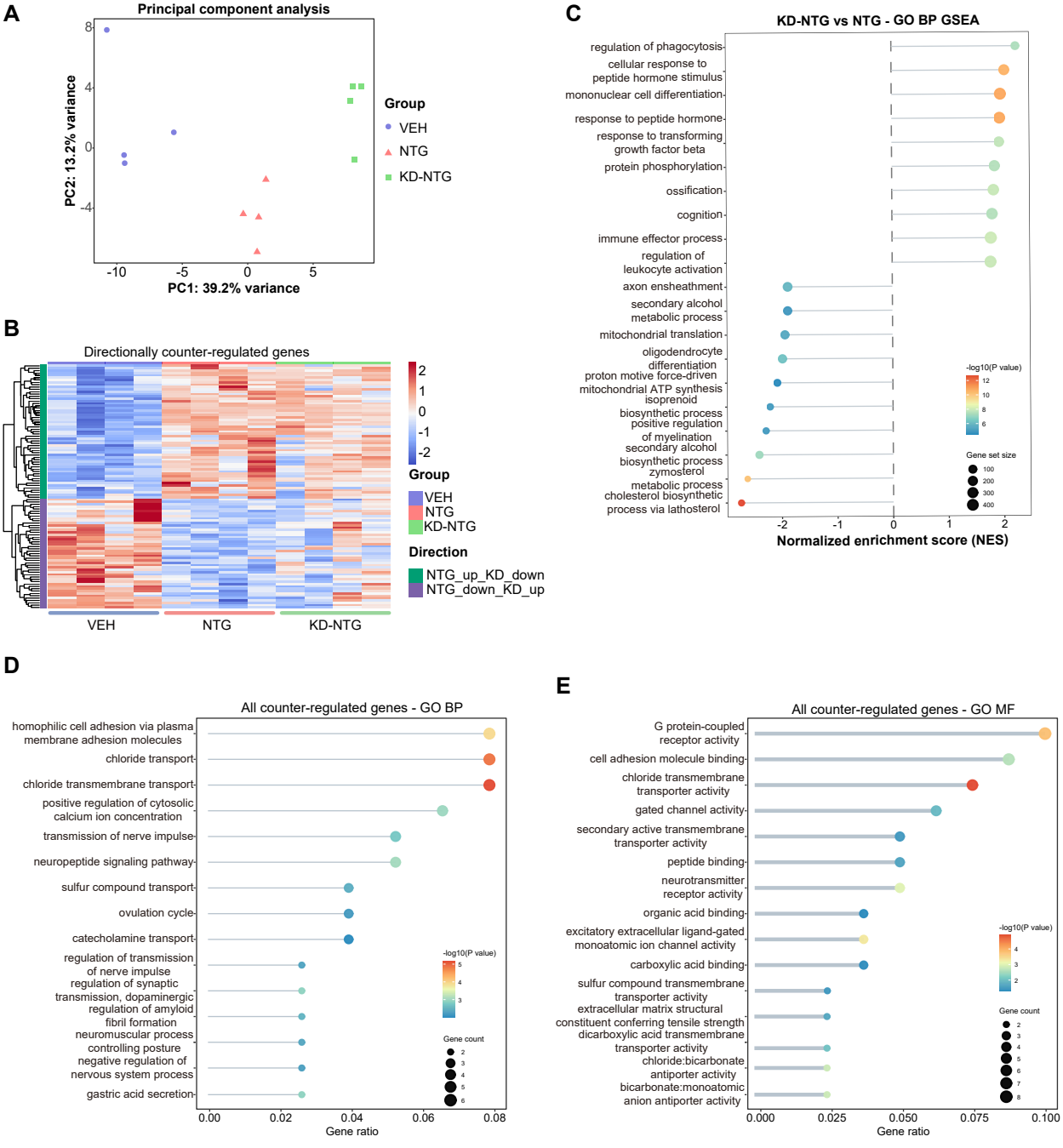
A
Principal component analysis
PC2: 13.2% variance
PC1: 39.2% variance
Group
VEH
NTG
KD-NTG
B
Directionally counter-regulated genes
Group
VEH
NTG
KD-NTG
Direction
NTG_up_KD_down
NTG_down_KD_up
C
KD-NTG vs NTG - GO BP GSEA
regulation of phagocytosis
cellular response to peptide hormone stimulus
mononuclear cell differentiation
response to peptide hormone
response to transforming growth factor beta
protein phosphorylation
ossification
cognition
immune effector process
regulation of leukocyte activation
axon ensheathment
secondary alcohol metabolic process
mitochondrial translation
oligodendrocyte differentiation
proton motive force-driven mitochondrial ATP synthesis
isoprenoid biosynthetic process
positive regulation of myelination
secondary alcohol biosynthetic process
zymosterol metabolic process
cholesterol biosynthetic process via lathosterol
-log10(P value)
Gene set size
Normalized enrichment score (NES)
D
All counter-regulated genes - GO BP
homophilic cell adhesion via plasma membrane adhesion molecules
chloride transport
chloride transmembrane transport
positive regulation of cytosolic calcium ion concentration
transmission of nerve impulse
neuropeptide signaling pathway
sulfur compound transport
ovulation cycle
catecholamine transport
regulation of transmission of nerve impulse
regulation of synaptic transmission, dopaminergic
regulation of amyloid fibril formation
neuromuscular process controlling posture
negative regulation of nervous system process
gastric acid secretion
-log10(P value)
Gene count
Gene ratio
E
All counter-regulated genes - GO MF
G protein-coupled receptor activity
cell adhesion molecule binding
chloride transmembrane transporter activity
gated channel activity
secondary active transmembrane transporter activity
peptide binding
neurotransmitter receptor activity
organic acid binding
excitatory extracellular ligand-gated monoatomic ion channel activity
carboxylic acid binding
sulfur compound transmembrane transporter activity
extracellular matrix structural constituent conferring tensile strength
dicarboxylic acid transmembrane transporter activity
chloride:bicarbonate antiporter activity
bicarbonate:monoatomic anion antiporter activity
-log10(P value)
Gene count
Gene ratio

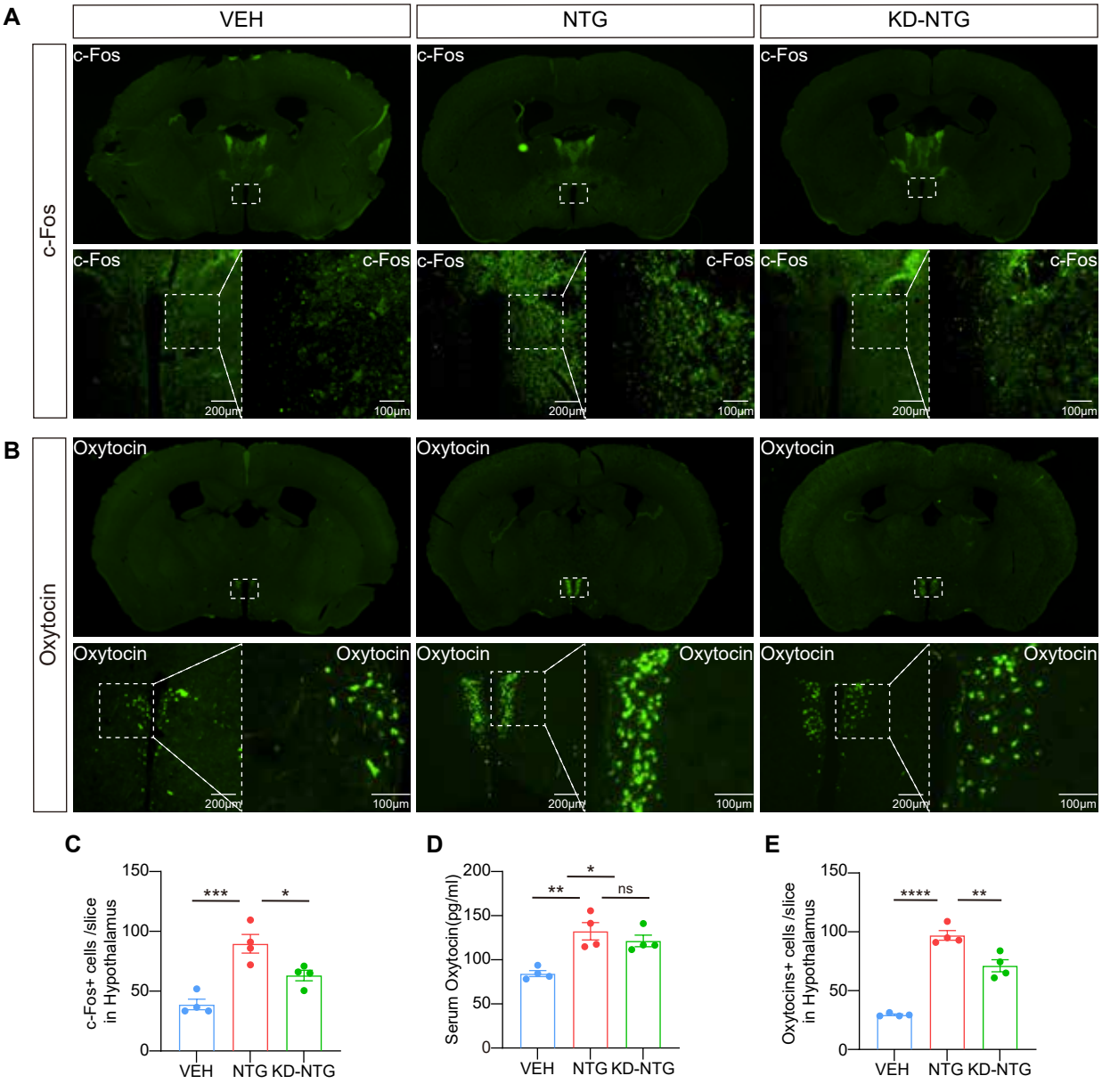
A
VEH
NTG
KD-NTG
c-Fos
c-Fos
c-Fos
c-Fos
c-Fos
c-Fos
c-Fos
c-Fos
c-Fos
200μm
100μm
200μm
100μm
200μm
100μm
B
Oxytocin
Oxytocin
Oxytocin
Oxytocin
Oxytocin
Oxytocin
Oxytocin
Oxytocin
Oxytocin
200μm
100μm
200μm
100μm
200μm
100μm
C
c-Fos+ cells /slice in Hypothalamus
150
100
50
0
***
*
VEH
NTG
KD-NTG
D
Serum Oxytocin(pg/ml)
200
150
100
50
0
**
*
ns
VEH
NTG
KD-NTG
E
Oxytocins+ cells /slice in Hypothalamus
150
100
50
0
****
**
VEH
NTG
KD-NTG

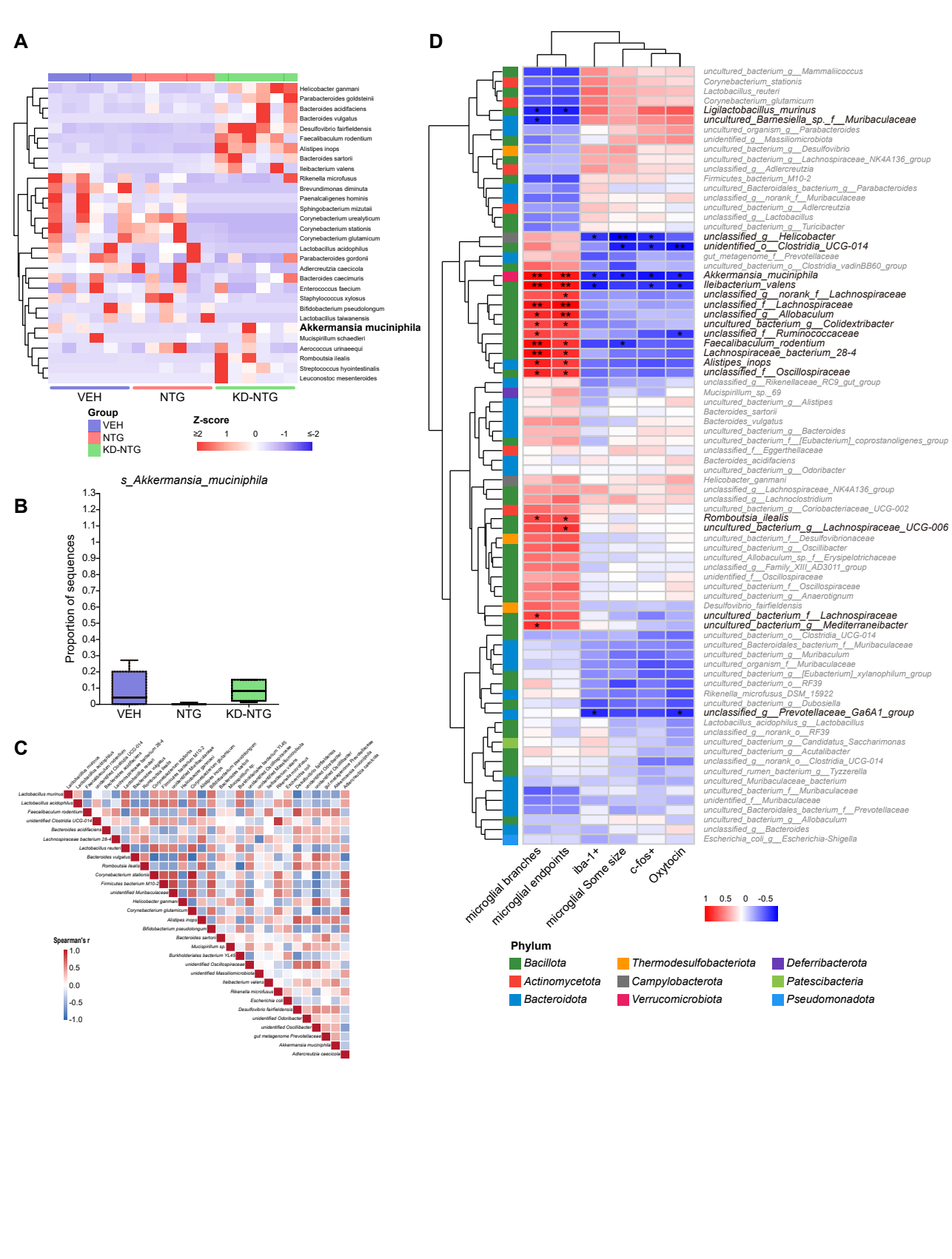
A
Helicobacter ganmani
Parabacteroides goldsteinii
Bacteroides acidifaciens
Bacteroides vulgatus
Desulfovibrio fairfieldensis
Faecalibaculum rodentium
Alistipes inops
Bacteroides sartorii
Ileibacterium valens
Rikenella microfusus
Brevundimonas diminuta
Paenalcaligenes hominis
Sphingobacterium mizutaii
Corynebacterium urealyticum
Corynebacterium stationis
Corynebacterium glutamicum
Lactobacillus acidophilus
Parabacteroides gordonii
Adlercreutzia caecicola
Bacteroides caecimuris
Enterococcus faecium
Staphylococcus xylosus
Bifidobacterium pseudolongum
Lactobacillus taiwanensis
Akkermansia muciniphila
Mucispirillum schaedleri
Aerococcus urinaeequi
Romboutsia ilealis
Streptococcus hyointestinalis
Leuconostoc mesenteroides
VEH
NTG
KD-NTG
Group
VEH
NTG
KD-NTG
Z-score
≥2
1
0
-1
≤-2
B
s_Akkermansia_muciniphila
Proportion of sequences
VEH
NTG
KD-NTG
C
Spearman's r
1.0
0.5
0.0
-0.5
-1.0
D
uncultured_bacterium_g__Mammaliicoccus
Corynebacterium_stationis
Lactobacillus_reuteri
Corynebacterium_glutamicum
Ligilactobacillus_murinus
uncultured_Barnesiella_sp._f__Muribaculaceae
uncultured_organism_g__Parabacteroides
unidentified_g__Massiliomicrobiota
uncultured_bacterium_g__Desulfovibrio
uncultured_bacterium_g__Lachnospiraceae_NK4A136_group
unclassified_g__Adlercreutzia
Firmicutes_bacterium_M10-2
uncultured_Bacteroidales_bacterium_g__Parabacteroides
unclassified_g__norank_f__Muribaculaceae
uncultured_bacterium_g__Adlercreutzia
unclassified_g__Lactobacillus
uncultured_bacterium_g__Turicibacter
unclassified_g__Helicobacter
unidentified_o__Clostridia_UCG-014
gut_metagenome_f__Prevotellaceae
uncultured_bacterium_o__Clostridia_vadinBB60_group
Akkermansia_muciniphila
Ileibacterium_valens
unclassified_g__norank_f__Lachnospiraceae
unclassified_f__Lachnospiraceae
unclassified_g__Allobaculum
uncultured_bacterium_g__Colidextribacter
unclassified_f__Ruminococcaceae
Faecalibaculum_rodentium
Lachnospiraceae_bacterium_28-4
Alistipes_inops
unclassified_f__Oscillospiraceae
unclassified_g__Rikenellaceae_RC9_gut_group
Mucispirillum_sp._69
uncultured_bacterium_g__Alistipes
Bacteroides_sartorii
Bacteroides_vulgatus
uncultured_bacterium_g__Bacteroides
uncultured_bacterium_f__[Eubacterium]_coprostanoligenes_group
unclassified_f__Eggerthellaceae
Bacteroides_acidifaciens
uncultured_bacterium_g__Odoribacter
Helicobacter_ganmani
unclassified_g__Lachnospiraceae_NK4A136_group
unclassified_g__Lachnoclostridium
uncultured_bacterium_g__Coriobacteriaceae_UCG-002
Romboutsia_ilealis
uncultured_bacterium_g__Lachnospiraceae_UCG-006
uncultured_bacterium_f__Desulfovibrionaceae
uncultured_bacterium_g__Oscillibacter
uncultured_Allobaculum_sp._f__Erysipelotrichaceae
unclassified_g__Family_XIII_AD3011_group
unidentified_f__Oscillospiraceae
uncultured_bacterium_f__Oscillospiraceae
uncultured_bacterium_g__Anaerotignum
Desulfovibrio_fairfieldensis
uncultured_bacterium_f__Lachnospiraceae
uncultured_bacterium_g__Mediterraneibacter
uncultured_bacterium_o__Clostridia_UCG-014
uncultured_Bacteroidales_bacterium_f__Muribaculaceae
uncultured_bacterium_g__Muribaculum
uncultured_organism_f__Muribaculaceae
uncultured_bacterium_g__[Eubacterium]_xylanophilum_group
uncultured_bacterium_o__RF39
Rikenella_microfusus_DSM_15922
uncultured_bacterium_g__Dubosiella
unclassified_g__Prevotellaceae_Ga6A1_group
Lactobacillus_acidophilus_g__Lactobacillus
unclassified_g__norank_o__RF39
uncultured_bacterium_g__Candidatus_Saccharimonas
uncultured_bacterium_g__Acutalibacter
unclassified_g__norank_o__Clostridia_UCG-014
uncultured_rumen_bacterium_g__Tyzzerella
uncultured_Muribaculaceae_bacterium
uncultured_bacterium_f__Muribaculaceae
unidentified_f__Muribaculaceae
uncultured_Bacteroidales_bacterium_f__Prevotellaceae
uncultured_bacterium_g__Allobaculum
unclassified_g__Bacteroides
Escherichia_coli_g__Escherichia-Shigella
microglial branches
microglial endpoints
iba-1+
microglial Some size
c-fos+
Oxytocin
1
0.5
0
-0.5
Phylum
Bacillota
Actinomycetota
Bacteroidota
Thermodesulfobacteriota
Campylobacterota
Verrucomicrobiota
Deferribacterota
Patescibacteria
Pseudomonadota

Supplementary Files

This is a list of supplementary files associated with this preprint. Click to download.

- FIGs2.pdf
- figS1.pdf